

## **Release of IFN- $\gamma$ by acute myeloid leukemia cells remodels bone marrow immune microenvironment by inducing regulatory T cells**

Giulia Corradi,<sup>1#</sup> Barbara Bassani,<sup>2#</sup> Giorgia Simonetti,<sup>3</sup> Sabina Sangaletti,<sup>2</sup> Jayakumar Vadakekolathu,<sup>4</sup> Maria Chiara Fontana,<sup>3</sup> Martina Pazzaglia,<sup>3</sup> Alessandro Gulino,<sup>5</sup> Claudio Tripodo,<sup>5</sup> Gianluca Cristiano,<sup>1</sup> Lorenza Bandini,<sup>6</sup> Emanuela Ottaviani,<sup>6</sup> Darina Ocadlikova<sup>1</sup>, Milena Piccioli<sup>8</sup>, Giovanni Martinelli,<sup>3</sup> Mario Paolo Colombo,<sup>2</sup> Sergio Rutella,<sup>4,7</sup> Michele Cavo,<sup>1,6</sup> Marilena Ciciarello\*<sup>9,10,11</sup> and Antonio Curti\*<sup>6</sup>

<sup>1</sup>Dipartimento di Medicina Specialistica, Diagnostica e Sperimentale, Università di Bologna, Bologna, Italy; <sup>2</sup>Fondazione IRCCS, Istituto Nazionale dei Tumori, Milan, Italy; <sup>3</sup>IRCCS Istituto Romagnolo per lo Studio dei Tumori "Dino Amadori"-IRST, Meldola (FC), Italy; <sup>4</sup>John van Geest Cancer Research Centre, College of Science and Technology, Nottingham Trent University, Nottingham, UK; <sup>5</sup>Tumor Immunology Unit, Department of Health Sciences, University of Palermo, Palermo, Italy; <sup>6</sup>IRCCS Azienda Ospedaliero-Universitaria di Bologna, Istituto di Ematologia "Seràgnoli", Bologna, Italy; <sup>7</sup>Centre for Health, Ageing and Understanding Disease (CHAUD), Nottingham Trent University Clifton Campus, Nottingham, UK; <sup>8</sup>Haematopathology Unit, IRCCS Azienda Ospedaliero-Universitaria di Bologna, Bologna, Italy; <sup>9</sup>Istituto di Ematologia "Seràgnoli", Bologna, Italy; <sup>10</sup>CNR Institute of Molecular Genetics "Luigi Luca Cavalli-Sforza", Unit of Bologna, Bologna, Italy; <sup>11</sup>IRCCS Istituto Ortopedico Rizzoli, Bologna, Italy.

# G.C. and B.B. contributed equally to this study.

\* M. Ciciarello and A.C. contributed equally to this study.

**Running title:** IFN- $\gamma$  and leukemic microenvironment

**Keywords:** IFN- $\gamma$ , acute myeloid leukemia, leukemic microenvironment, regulatory T cells, stromal microenvironment

**Correspondence:** Prof. Michele Cavo, IRCCS Azienda Ospedaliero-Universitaria di Bologna, Istituto di Ematologia "Seràgnoli", Dipartimento di Medicina Specialistica, Diagnostica e Sperimentale, Università di Bologna

Via Massarenti 9, 40138 Bologna, Italy. Tel: +39-0512143809, +39-0512143537; Fax: +39-051398973; e-mail: [michele.cavo@unibo.it](mailto:michele.cavo@unibo.it)

### **Authors' Disclosures**

The authors declare no potential conflicts of interest.

## **Translational significance**

In most tumors, IFN- $\gamma$  provides a signal resulting in enhanced anti-tumor immunity and better clinical outcome. By contrast, our study reveals the “dark side” of IFN- $\gamma$  in the creation of an immune-tolerant microenvironment enriched in Tregs and correlated with a worse prognosis in AML patients. *In vitro* and *in vivo* results demonstrate that IFN- $\gamma$  released by AML cells, not by leukemia-infiltrating immune cells, remodels the BM immune and stromal microenvironment by inducing suppressive Tregs. Given the emerging role of immunotherapies for AML, our findings support the incorporation of a new panel of microenvironment-based immunological factors into current AML classification and prognostication systems. Moreover, a greater understanding of the IFN- $\gamma$ -dependent tolerogenic tuning of the BM microenvironment provides the rationale for therapies targeting IFN- $\gamma$ -driven immune-modulatory effects on stromal and immune AML microenvironment, i.e., IDO1 inhibitors, and combining the activation of effector cells with the inhibition of Tregs.

## **Abstract**

**Purpose:** The stromal and immune bone marrow (BM) landscape is emerging as a crucial determinant for acute myeloid leukemia (AML). Regulatory T cells (Tregs) are enriched in the AML microenvironment, but the underlying mechanisms are poorly elucidated. Here, we addressed the effect of IFN- $\gamma$  released by AML cells in BM Tregs induction and its impact on AML prognosis.

**Experimental design:** BM aspirates from AML patients were subdivided according to *IFNG* expression. Gene expression profiles in *IFNG*<sup>high</sup> and *IFNG*<sup>low</sup> samples were compared by microarray and NanoString analysis and used to compute a prognostic index. The IFN- $\gamma$  release effect on the BM microenvironment was investigated in mesenchymal stromal cell (MSC)/AML cell co-cultures. In mice, AML cells silenced for IFN- $\gamma$  expression were injected intrabone.

**Results:** *IFNG*<sup>high</sup> AML samples showed an upregulation of inflammatory genes, usually correlated with a good prognosis in cancer. By contrast, in AML patients, high *IFNG* expression associated

with poor overall survival. Notably, IFN- $\gamma$  release by AML cells positively correlated with a higher BM suppressive Tregs' frequency. In co-culture experiments, IFN $\gamma^{\text{high}}$  AML cells modified MSC transcriptome by up-regulating IFN- $\gamma$ -dependent genes related to Treg induction, including indoleamine 2,3-dioxygenase 1 (IDO1). IDO1 inhibitor abrogated the effect of IFN- $\gamma$  release by AML cells on MSC-derived Treg induction. *In vivo*, the genetic ablation of IFN- $\gamma$  production by AML cells reduced MSC IDO1 expression and Treg infiltration, hindering AML engraftment.

**Conclusions:** IFN- $\gamma$  release by AML cells induces an immune-regulatory program in MSCs and remodels BM immunological landscape toward Treg induction, contributing to an immunotolerant microenvironment.

## **Introduction**

Acute myeloid leukemia (AML) is a heterogeneous clonal disease that develops from a rare population of bone marrow leukemic stem cells (1). For many years, cytogenetic and molecular aberrations in hematopoietic stem cells were considered the only causative factors in AML onset and development. Recently, this notion has been challenged, and it is now established that AML pathophysiology also depends on the bone marrow (BM) microenvironment (2,3).

A component of the BM microenvironment that is crucial to AML pathophysiology is the immunological landscape (4,5). Aberrant cytokine production and a profound dysregulation of the frequency and function of immune cell subsets induce an immunosuppressive milieu, which favors the escape of AML cells from immune control (5,6). In particular, the BM microenvironment in AML is enriched in regulatory T cells (Tregs) (7,8), which contribute to the immunosuppressive phenotype (9), chemoresistance, and disease relapse (7,10). The induction and the suppressive functions of Tregs are regulated, among others, by mesenchymal stromal cells (MSCs) (11), recognized as pivotal contributors to the hematopoietic stem cell niche (12). A crucial mediator of MSC-driven Treg induction is indoleamine 2,3-dioxygenase 1 (IDO1) (13,14), a well-known tryptophan metabolizing enzyme contributing to the immunosuppressive tumor microenvironment (15,16). Notably, MSCs are not constitutively immunosuppressive but rather acquire this capacity, including the ability to induce Tregs, in response to pro-inflammatory stimuli (13,14).

Inflammation has recently emerged as a hallmark of cancer (17). Along with its pro-tumorigenic effects, inflammatory signals also influence the host immune response inhibiting tumor development (18). One such signal is interferon (IFN)- $\gamma$ , a cytokine produced predominantly by T cells and natural killer (NK) cells that suppresses hematopoiesis and is a master regulator of innate and adaptive immunity (19,20). In the tumor microenvironment, IFN- $\gamma$  orchestrates an array of anti-proliferative, pro-apoptotic, anti-tumor, immune-activating responses (21). IFN-related gene

signature is a favorable predictive marker for chemotherapy and radiotherapy efficiency as well as immunotherapy in various types of malignancies (22). However, emerging and seemingly paradoxical findings indicate that IFN- $\gamma$  can also be involved in pathways supporting tumorigenesis and immune evasion (23).

This study aimed to address whether IFN- $\gamma$  regulates immunological changes of the BM microenvironment in AML. For this purpose, we used BM aspirates from AML patients, cell-culture systems, and a murine AML model to investigate the ability of AML cells to favor the establishment of a Treg-centered immunosuppressive microenvironment through the release of IFN- $\gamma$ .

## **Materials and Methods**

### **Ethics statement**

This study is part of ongoing research approved by the Independent Ethics Committee of the Area Vasta Emilia Centro (94/2016/O/Tess). AML patients and healthy BM donors were recruited at Seràgnoli Hematology Institute in Bologna. Clinical samples and data were collected with written informed consent. The investigations were conducted in accordance with the Declaration of Helsinki.

### **Biological samples and cell cultures**

BM aspirate samples were collected from 49 AML patients at diagnosis (blasts  $\geq 80\%$ ) and 8 healthy donors (Supplementary Table S1) and used to isolate mononuclear cells (MNCs). BM aspirates were centrifuged over a Ficoll-Paque gradient (Lympholyte CL5020, Cedarlane). MNCs were collected, resuspended in RPMI 1640 medium (Lonza) with 10% fetal bovine serum (FBS) (Thermo Fisher Scientific), 2 mM L-glutamine (Gibco), 500 IU/ml penicillin, and 0.5 mg/ml streptomycin (Pen-strep, MP Biomedicals) (called RPMI complete culture medium), and frozen for further experiments.

Throughout the text, we referred to IFN- $\gamma^{\text{high}}$  or IFN- $\gamma^{\text{low}}$  AML cells as BM cells in the large majority ( $\geq 80\%$ ) expressing blast cell-associated markers and co-expressing IFN- $\gamma$ , respectively above or below the median within our AML patients' cohort.

BM samples were also used to isolate mesenchymal stromal cells (MSCs) as previously described (24). Briefly, MNCs were plated at  $1.6 \times 10^5$  cells/cm<sup>2</sup> in DMEM (Lonza), 10% FBS, 2 mM L-glutamine, 500 IU/ml penicillin and 0.5 mg/ml streptomycin (called DMEM complete culture medium). After 2-3 days, the non-adherent fraction was removed by rinsing with phosphate-buffered saline (PBS) and adherent cells were cultured until 70–80% confluence. Then, cells were

detached with 0.05% trypsin-EDTA with phenol red (Thermo Fisher Scientific), re-seeded at  $3.5 \times 10^3$  cells/cm<sup>2</sup>, and used for experiments within passages 3-5.

CD34<sup>+</sup> cells were purified from BM-derived MNCs from healthy donors by immunomagnetic separation (Miltenyi Biotec).

Healthy donor blood (buffy coats) was used for isolating peripheral blood mononuclear cells (PBMCs).

### **GeneChip gene expression profiling**

The first part of the study used gene expression data generated for our previous studies, specifically from BM mononuclear cells of 61 AML patients (blasts  $\geq 80\%$ ) (GSE161532) (25,26) (Supplementary Table S2) and 7 healthy BM donors (not previously reported). The patients include 29 men and 32 women of mean age 60.1 (SD = 11.9) years. In all cases, mononuclear cells had been isolated from BM aspirates by density gradient centrifugation and lysed in RLT buffer (Qiagen). RNA was extracted and reverse-transcribed into cDNA as previously reported (26). cDNA was hybridized to GeneChip Human Transcriptome Assay 2.0 microarrays (Thermo Fisher Scientific). Data were analyzed using Transcriptome Analysis Console 4.0 software (Thermo Fisher Scientific) and the SST-RMA (signal space transformation – robust multiple-array average) algorithm.

GeneChip data for *IFNG* mRNA were used to dichotomize the AML cell preparations into an IFNG<sup>low</sup> group (below the median) and IFNG<sup>high</sup> group (above the median). Then, for all genes, fold change (FC) in expression was calculated as IFNG<sup>high</sup>/IFNG<sup>low</sup>. Genes with  $|FC| \geq 2.0$  and  $P \leq 0.05$  (according to Transcriptome Analysis Console software) were considered differentially expressed. A heatmap of differentially expressed genes (DEGs) was generated using ClustVis (SCR\_017133)(27). DEGs were attributed to macro-pathways according to pathway analysis and

functional annotation (GeneCards, SCR\_002773) and analyzed using Enrichr (<https://amp.pharm.mssm.edu/Enrichr/>; SCR\_001575)(28).

### **Amplification-free gene expression profiling**

Messenger RNA was extracted from BM mononuclear cells of 24 AML patients (18 men and 6 women; mean age, 53.4 years; SD=17.6 years) (Supplementary Table S1) using Maxwell RSC simplyRNA Blood Kit (Promega). Samples (100-150 ng) were analyzed on the nCounter FLEX system using the PanCancer IO 360 Panel (NanoString Technologies). Reporter probe counts were analyzed using nSolver software (v4.0.62) and nSolver Advanced Analysis module (v2.0.115). Captured transcript counts were normalized to the geometric mean of the included reference genes and internal positive controls. DEGs between IFN $\gamma^{\text{high}}$  and IFN $\gamma^{\text{low}}$  groups (based on qRT-PCR) were identified using  $|\log_2 \text{FC}| > 2.0$  and  $P < 0.05$  (Benjamini–Yekutieli false discovery rate, Student's  $t$  test). The nSolver software package was used to calculate, for each sample, biological activity, and pathway scores, as linear combinations of pre-defined gene sets. STRING (<https://string-db.org/>; SCR\_005223) was used to analyze functional interaction networks.

### **Co-culture experiments**

To study the effects of AML cells on BM-derived MSCs, we used two-chamber co-cultures with MSCs in the lower and AML cells in the upper chamber. MSCs were seeded at  $2 \times 10^4$  cells/cm<sup>2</sup> in 6- or 24-well dishes in DMEM complete culture medium. After 24 h, hanging cell culture inserts (Millicell MCHT06H48, MCHT24H48, Millipore) were positioned for the seeding of IFN- $\gamma^{\text{high}}$  or IFN- $\gamma^{\text{low}}$  AML cells at  $1 \times 10^6$  cells/ml (ratio, 1:10 with MSCs), and cells were co-cultured for up to 4 days and recovered for analyses described below. MSCs cultured alone served as control. Co-cultures did not use matched pairs of MNCs and MSCs from the same BM aspirate.

*Gene expression profiling.* After 24 h of co-culture, MSCs (5 cultured with IFN- $\gamma^{\text{high}}$  AML cells, 4 with IFN- $\gamma^{\text{low}}$  AML cells, and 5 monocultures) were lysed in Trizol (Thermo Fisher Scientific). RNA was extracted in phenol-chloroform and converted into cDNA, which was profiled with

Clariom S Array gene expression assays (Thermo Fisher Scientific) and analyzed as described above. Differentially expressed genes (DEGs) between the two co-cultures and the MSC monoculture were identified using a  $|FC| \geq 2.0$  and  $P \leq 0.05$  (according to Transcriptome Analysis Console software). DEGs with known roles in the immune response were plotted in a heatmap reporting the ratio in expression level between MSCs+AML cells and MSCs alone for each sample. Genes were sorted by average linkage hierarchical clustering using ClustVis (27). Pathway enrichment analysis was performed using Enrichr (<https://amp.pharm.mssm.edu/Enrichr/>; SCR\_001575)(28) and Reactome, KEGG (SCR\_012773), and Gene Ontology-Biological Processes (GO-BP) annotations. Gene set enrichment analysis (GSEA; SCR\_003199) was performed with GSEA software (Broad Institute)(29), using  $q(\text{FDR}) \leq 0.05$  as cut-off for significance.

*Interferon- $\gamma$  and IDO1 analyses.* After 24 h of co-culture, the conditioned medium was collected, centrifuged to remove debris, and stored at  $-20^\circ\text{C}$  until analysis of IFN- $\gamma$  using the IFN gamma Human ProQuantum Immunoassay Kit (Thermo Fisher Scientific). After 4 days of co-culture, MSCs were recovered and processed for qRT-PCR of *IFNG* and *IDO1* mRNA, flow cytometry of IFN- $\gamma^+$  and IDO1 $^+$  cells, and western blotting of IDO1. Where indicated, IFN- $\gamma^{\text{high}}$  and IFN- $\gamma^{\text{low}}$  AML cells were recovered after co-cultures and processed for qRT-PCR and flow cytometry.

*In vitro Treg assays.* For this set of experiments, PBMCs were obtained from buffy coats after centrifugation over a Ficoll-Paque gradient. IFN- $\gamma^{\text{high}}$  AML cells were co-cultured with MSCs. After 4 days of co-culture, IFN- $\gamma^{\text{high}}$  AML cells were removed and replaced with PBMCs seeded at  $1 \times 10^6$  cells/ml (ratio, 1:10 with MSCs). After 7 days, PBMCs were recovered and stained with monoclonal antibodies (mAbs) (Supplementary Table S7) using the FoxP3/Transcription Factor Staining Buffer Set (Thermo Fisher Scientific). At least 10,000 events were analyzed by flow cytometry. CD3 $^+$ CD4 $^+$ CD25 $^+$ FOXP3 $^+$  cells were gated on CD4 $^+$  cells.

For a Treg suppression assay, after 7 days of co-culture with IFN- $\gamma^{\text{high}}$  AML cell-primed MSCs, PBMCs were recovered. CD4<sup>+</sup>CD25<sup>+</sup> cells were magnetically purified from PBMCs and co-cultured with autologous CD3<sup>+</sup> cells (ratio, 1:10), labeled with 1  $\mu$ M carboxyfluorescein succinimidyl ester (CFSE, Abcam). Briefly, CD3<sup>+</sup> were washed twice in PBS, incubated with CFSE in the dark at 37° C for 10 minutes, and washed twice in RPMI complete culture medium. The proliferation of CD3<sup>+</sup> was stimulated by anti-CD3 and anti-CD28 beads (ExpAct™ Treg Kit, Miltenyi Biotec), and was considered as a positive control. CD4<sup>+</sup>CD25<sup>-</sup> T cells were used as negative effector cells. Cell proliferation was monitored after 4 days of culture, analyzing CFSE dye dilution by flow cytometry. The proliferation index was calculated using FCS Express 4 software (De Novo Software, Milan, Italy).

For suppression assay with Treg from IFN- $\gamma^{\text{high}}$  AML patients, CD3<sup>+</sup> cells, CD4<sup>+</sup>CD25<sup>+</sup> and CD4<sup>+</sup>CD25<sup>-</sup> were magnetically purified from BM-derived MNCs isolated from IFN- $\gamma^{\text{high}}$  AML patients. The experiments were performed as described above.

For a Treg conversion assay, CD4<sup>+</sup>CD25<sup>-</sup> cells were isolated from PBMCs by immunomagnetic separation (CD4<sup>+</sup>CD25<sup>+</sup> Regulatory T Cell Isolation kit, Miltenyi Biotec). IFN- $\gamma^{\text{high}}$  AML cells were co-cultured with MSCs. After 4 days, IFN- $\gamma^{\text{high}}$  AML cells were removed and replaced with CD4<sup>+</sup>CD25<sup>-</sup> cells seeded at 1x10<sup>6</sup> cells/ml (ratio, 1:10 with MSCs) and cultured in the absence or presence of the IDO1 inhibitor 1-methyl-DL-tryptophan (1 mM final concentration, Sigma Aldrich). In parallel, CD4<sup>+</sup>CD25<sup>-</sup> cells were seeded with IFN- $\gamma^{\text{high}}$  AML cells without MSCs. After 7 days, non-adherent cells were recovered, and stained with mAbs (Supplementary Table S7); the percentage of CD4<sup>+</sup>CD25<sup>+</sup>FOXP3<sup>+</sup> cells was analyzed by flow cytometry.

For a Treg proliferation assay, IFN- $\gamma^{\text{high}}$  AML cells and MSCs were co-cultured for 4 days. On the fourth day, PBMCs were labeled with 1  $\mu$ M CFSE (Abcam) as described above. The IFN- $\gamma^{\text{high}}$  AML cells of the co-cultures were replaced with labeled PBMCs. After 7 days, PBMCs were recovered and stained as described above, and the CD4<sup>+</sup>CD25<sup>+</sup> cell proliferation was determined by

flow cytometry. The proliferation index was calculated using FCS Express 4 software (De Novo Software, Milan, Italy).

*IFN- $\gamma$ -inactivation.* MSCs were cultured for 6 h, alone or with IFN- $\gamma^{\text{high}}$ / IFN- $\gamma^{\text{low}}$  AML cells in the absence or presence of 20  $\mu\text{g/ml}$  anti-human IFN- $\gamma$  (NIB42, BD Pharmingen; AB\_395471) or 10  $\mu\text{g/ml}$  anti-human IFN- $\gamma\text{R}$  (GIR-208, BD Pharmingen; AB\_396745). MSCs were recovered and processed for qRT-PCR of *IDO1* mRNA.

### **Induction of IDO1 expression**

MSCs from healthy BM donors or AML patients were seeded at  $3.5 \times 10^3$  cells/cm<sup>2</sup> and, after 24 h, IFN- $\gamma$  (50 ng/ml; Thermo Fisher Scientific), tumor necrosis factor  $\alpha$  (10 ng/ml; Endogen), interleukin 6 (10 ng/ml; Endogen) or prostaglandin E2 (1  $\mu\text{g/ml}$ ; Endogen) was added to the medium. After 24 h, cells were harvested and analyzed for *IDO1* mRNA expression by qRT-PCR.

### **Quantitative real-time PCR**

For the analysis of human samples, cells were lysed in RLT Plus buffer (Qiagen); mRNA was isolated using RNeasy Micro kits (Qiagen), quantified by spectrophotometry (ND-1000, NanoDrop Technologies), and reverse-transcribed into cDNA using the ImProm-II kit (Promega). For the analysis of murine samples, cells were lysed in RNA lysis buffer (Zymo Research); mRNA was isolated using Quick RNA micro prep kit (Zymo Research), quantified by spectrophotometry, and reverse-transcribed using the MultiScribe reverse transcriptase (Thermo Fisher Scientific).

qRT-PCR reactions were performed using a 96-well Optical Reaction Plate. Amplification reactions using human cDNA were done using Platinum Super mix (Thermo Fisher Scientific), and those using murine cDNA with TaqMan Fast Universal PCR Master Mix (Thermo Fisher Scientific). Primer probes used for target genes are listed in Supplementary Table S8. Threshold cycle ( $C_t$ ) values were determined automatically using the 7900HT Fast Real-Time PCR system (Applied Biosystems). Relative quantification was performed using the  $\Delta C_t$  comparative method (30). Where

indicated, cDNA reverse-transcribed from Universal Human Reference RNA (Agilent) was used as the control.

### **Western blotting**

Cells were lysed in Cell Lysis Buffer (Cell Signaling Technology) with 1 mM phenylmethanesulfonyl fluoride (Sigma Aldrich) according to the manufacturer's protocol. Protein (40 µg per sample) was separated on 12% polyacrylamide gels (Mini-PROTEAN TGX Stain-Free Precast Gels, Bio-Rad), transferred to nitrocellulose membranes, and incubated overnight at 4 °C with primary and secondary antibodies (Supplementary Table S7). Bound antibodies were revealed by chemiluminescence (Amersham ECL Select, GE Healthcare).

### **Murine model of AML**

Animal studies were approved by the Committee for Animal Welfare of Fondazione IRCCS Istituto Nazionale dei Tumori and Italian Ministry of Health (authorization 781/2018-PR) and performed following Italian law D.lgs 26/2014.

C57BL/6 male and female mice (age, 8-12-weeks) were obtained from Charles River Italia (Calco, Italy). The C1498 (TIB-49) murine acute leukemia cell line was obtained from ATCC (CVCL\_3494) and the WEHI 3B murine myelomonocyte cell line was from Sigma Aldrich (CVCL\_2239). Cell lines were cultured at 37°C in fully humidified atmosphere with 5% CO<sub>2</sub> and were monthly checked for Mycoplasma using MycoAlert Mycoplasma detection Kitt (Lonza).

To create a murine model of AML, the murine acute leukemia cell line C1498 was infected with lentiviral particles containing the vector pGFP-C-sh expressing either *Ifnγ*-specific interfering shRNA (shIFN-γ) or non-specific shRNA (control cells) (TL501051V, OriGene Technologies). Infected cells were cultured for 2 weeks before injection into the tibias of C57BL/6 mice. Two weeks after infection, the percentages of GFP<sup>+</sup> cells were measured using a LSRFortessa flow cytometer (BD), and GFP<sup>+</sup> cells were selected by fluorescence-activated cell sorting on a FACS Aria

flow cytometer (BD). The proliferation of control-C1498-GFP<sup>+</sup> (control) and shIFN $\gamma$ -C1498-GFP<sup>+</sup> cell (called shIFN- $\gamma$  cells) was evaluated using the Cell Proliferation Kit (XTT) (Sigma Aldrich), and formazan products were detected by absorbance at 450 nm (Tecan's Spark Microplate reader, reference wavelength, 670 nm). Control and shIFN- $\gamma$  cell apoptosis was evaluated by flow cytometry using the 7-AAD/Annexin V staining after 24h, 48h, and 72h of culture.

For in vivo experiments,  $2 \times 10^5$  shIFN- $\gamma$  cells or control cells were injected intra-bone in the tibia of age and sex-matched C57BL/6. After 31 days, mice were sacrificed, tibia were retrieved and the BM was flushed with 2% FBS, 2 mM EDTA in PBS. Engraftment was estimated as the percentage of GFP<sup>+</sup> cells in the tibial wash, determined by flow cytometry. This experiment was performed twice, and data are reported as the mean and SEM.

In IDO1-inhibition experiments, control-C1498-GFP<sup>+</sup> were injected and, after 15 days, twice-weekly treatment was started with NLG919 (50 mg/kg i.p., Abcam). Mice were killed at day 31 for flow cytometry of BM.

### **Flow cytometry**

Antibodies used for flow cytometry are indicated in Supplementary Table S7. For surface staining,  $0.5 \times 10^6$  MNCs were washed in 0.5% FBS in PBS, and labeled with a dye-conjugated antibody by incubation at room temperature in the dark for 15 min. For intracellular staining, at least  $1 \times 10^5$  MNCs or MSCs were fixed and permeabilized using the Cytofix/Cytoperm Kit (BD Biosciences), and labeled with a dye-conjugated antibody at 4 °C in the dark for 30 min. Intracellular staining of Tregs was done using the Foxp3/Transcription Factor Staining Buffer Kit (Thermo Fisher Scientific and Tonbo Biosciences). In murine experiments, total BM-derived cells were analyzed.

Human cells were analyzed on a FACScanto II flow cytometer (BD) using FACSDiva (BD)(SCR\_001456) and FCS Express 4 software. Cell autofluorescence was used as the negative control. Murine cells were analyzed on a FACSCelesta flow cytometer with FACSDiva and FlowJo

(v10. 2) software (SCR\_008520). The IFN- $\gamma^{\text{high}}$  samples were identified as having a percentage of IFN- $\gamma^+$  cells above the median value of all AML samples analyzed by flow cytometry. AML cells were identified as being CD34<sup>+</sup>, CD33<sup>+</sup>, or CD117<sup>+</sup> according to the phenotype established at diagnosis. NK cells were identified as CD3<sup>-</sup>CD45<sup>+</sup>CD56<sup>+</sup> cells. Fluorescence minus one (FMO) control was preliminarily performed (not shown). Human BM-derived total Tregs were identified as CD3<sup>+</sup>CD4<sup>+</sup>CD25<sup>+</sup>CD127<sup>low/-</sup> cells, and the activated subset of Tregs was identified as CD25<sup>high</sup>CD45RA<sup>-</sup>FOXP3<sup>+</sup> within the total Treg population, and gated on CD4<sup>+</sup> cells (see the gating strategy in Supplementary Figure S2E).

### **Immunohistochemistry and immunofluorescence**

Mouse tibia were decalcified using an EDTA-based decalcifying solution (MicroDec, Diapath) and embedded in paraffin. Sections (4  $\mu\text{m}$ ) were deparaffinized, rehydrated and unmasked using the Epitope Retrieval Solution pH 9 (Novocastra) at 98 °C for 30 min. After neutralization of endogenous peroxidase and Fc blocking (Novocastra), samples were incubated with antibodies listed in Supplementary Table S7.

For immunohistochemistry, bound HRP-conjugated antibodies were revealed by staining with 3-amino-9-ethylcarbazole substrate-chromogen (Dako Agilent), and slides were counterstained with Harris hematoxylin (Novocastra). For immunofluorescence, fluorescent secondary antibodies were used (Supplementary Table S7) and nuclei were counterstained with 4',6-diamidino-2-phenylindole, dihydrochloride (DAPI). Slides were analyzed under an Axioscope A1 microscope equipped with an Axiocam 503 Color digital camera and Zen 2.0 software (Zeiss).

Quantification of IDO1 immunohistochemical staining was performed by calculating the average percentage of positive signals (3+ and 2+) in five non-overlapping fields at high-power magnification ( $\times 400$ ) using the Positive Pixel Count algorithm (Image Analysis Software v9, Leica). Quantification of IDO1 signal in immunofluorescence in  $\alpha\text{SMA-nestin}^+$  cells, was

performed by calculating the average percentage of IDO1 intensity in double positive cells in five non-overlapping fields with high power magnification (x400) using HALO (version v3.2.1851.229) Image analysis software.

### **Prognostic index**

A prognostic index (PI) was generated using the method of Wagner et al.(31) using  $\beta$  values from Cox regression analyses of the 30 DEGs between IFNG<sup>high</sup> and IFNG<sup>low</sup> samples. The index was calculated for 149 adults with non-promyelocytic AML (enrolled in Cancer and Leukemia Group B treatment protocols 8525, 8923, 9621, 9720, 10201, and 19808) for whom data on survival and gene expression were generated by The Cancer Genome Atlas (TCGA) Research Network: <https://www.cancer.gov/tcga>. Overall survival was computed from the date of diagnosis to the date of death. Patients were dichotomized at the median PI value, and the log-rank (Mantel-Cox) test was used to compare survival curves.

### **Data availability**

For the original gene expression data, please contact: [giorgia.simonetti@irst.emr.it](mailto:giorgia.simonetti@irst.emr.it). For the original NanoString nCounter FLEX data, please contact: [sergio.rutella@ntu.ac.uk](mailto:sergio.rutella@ntu.ac.uk). Gene expression and NanoString data have been deposited in NCBI's Gene Expression Omnibus and are accessible through GEO Series accession numbers GSE161532 (AML)(25), GSE155441 (MSCs vs. AML/MSCs), and GSE146204 (NanoString).

### **Statistical analysis**

Tests used in statistical analyses are indicated in the figure legends.  $P < 0.05$  was considered significant. Analyses were done using GraphPad Prism software (v6.0; SCR\_002798).

## Results

### **IFNG<sup>high</sup> AML samples have a gene signature enriched in IFN- $\gamma$ signaling, inflammatory, and immune-response pathways, which correlates with poor clinical outcome**

To clarify the role of IFN- $\gamma$  signaling in AML, we first compared *IFNG* mRNA levels in BM aspirates of AML patients and healthy donors (**Fig. 1A**). From existing GeneChip microarray data, it emerged that *IFNG* mRNA levels in AML samples had a broad distribution skewed to higher values. The median was used to dichotomize AML samples into IFNG<sup>low</sup> and IFNG<sup>high</sup> groups (**Fig. 1B**). Expression levels in IFNG<sup>low</sup> and IFNG<sup>high</sup> groups were lower and higher, respectively, than in samples from healthy BM donors. Clinical characteristics of AML patients were similar in the IFNG<sup>high</sup> and IFNG<sup>low</sup> groups (Supplementary Table S2)(25,26), and no significant correlations with sex, age, WBC, karyotype, *FLT3*-ITD mutation, *NPM1* mutation, *FLT3*-internal tandem duplication (ITD) and *NPM1* mutation combination, and global risk (32) were found within the two groups.

To determine whether the groups of AML cells differed in overall gene expression, we used the same data to identify differentially expressed genes (DEGs) and found 47 up-regulated and 19 down-regulated genes in the IFNG<sup>high</sup> group compared to the IFNG<sup>low</sup> group (**Fig. 1C**, DataSheet\_page1). Ranking DEGs in macro-pathways revealed that 19 genes belonged to inflammation and immune response pathways. Notably, the IFNG<sup>high</sup> group had lower expression levels of genes involved in immune responses (e.g., *CIITA*, *CD180*, *CD1C*) and higher expression levels of genes involved in inflammation (e.g., *CXCL8*, *CCL4*, *CXCL2*). Enrichment analysis revealed that the DEGs were involved in IFN- $\gamma$  response pathways, including cytokine-mediated signaling, among other pathways (Supplementary Table S3). Since AML samples at median cut-off range in IFNG<sup>high</sup> and IFNG<sup>low</sup> groups have similar level of *IFNG* expression, we re-analyzed GEP, comparing samples in the top 3<sup>rd</sup> and the bottom 3<sup>rd</sup> percentile (Supplementary Fig. S1). We selected

21 patients, excluding 19 at the median cut-off. We found 141 DEG particularly enriched in genes belonging to immune response macro-pathway (123 up-regulated, 18 down-regulated, DataSheet\_page2). Enrichment analysis confirmed the modulation of immune/inflammation-related pathways (Supplementary Table S4).

To further investigate this phenomenon, we analyzed 24 BM samples of AML patients, from a cohort not overlapping with that of GeneChip microarray. qRT-PCR on *IFNG* mRNA was used to dichotomize samples into  $IFNG^{high}$  and  $IFNG^{low}$  groups. Samples classified as  $IFNG^{high}$  expressed significantly higher levels of *IFNG* mRNA than  $IFNG^{low}$  AML samples (Supplementary Fig. S2A). The expression of 750 cancer-related genes was profiled in an amplification-free manner on the nCounter platform using the PanCancer IO 360 Panel (NanoString).

These data were then used to detect DEGs between  $IFNG^{high}$  and  $IFNG^{low}$  groups. 30 DEGs were identified, 27 upregulated and 3 down-regulated genes in the  $IFNG^{high}$  group compared to the  $IFNG^{low}$  group (**Fig. 2A**, DataSheet\_page3). *CD28*, *CXCL8*, *GZMH*, *GZMA*, *IFIT1*, *CD8A*, and *CD3G* were among the most significantly up-regulated genes in  $IFNG^{high}$  samples, corroborating the relationship between high *IFNG* expression and modulated IFN- $\gamma$  signaling observed above (**Fig. 1C**; Supplementary Table S3). Two genes (i.e., *CXCL8*, *CD69*) out of 30 DEG in NanoString analysis resulted up-regulated in GeneChip analysis also. Both genes were upregulated in the  $IFNG^{high}$  cohort.

Pathway analysis revealed an enrichment of DEGs in KEGG pathways related to T cell receptor signaling, Th1 and Th2 cell differentiation, Wnt, and NF- $\kappa$ B signaling (Supplementary Table S5).

Network interaction analysis showed the DEGs involved in molecular pathways known to be enriched in solid cancers (Supplementary Fig. S2B).

We then used the DEGs to compute 25 biological activity and pathway scores (Supplementary Fig. S2C).  $IFNG^{high}$  samples expressed higher levels of genes belonging to PI3K-Akt, MAPK,

JAK/STAT, and NF- $\kappa$ B signaling pathways. In contrast, IFNG<sup>low</sup> samples had increased expression of gene sets reflecting epigenetic regulation, DNA damage repair, cellular proliferation, and autophagy.

Using NanoString data for all 24 samples, we examined correlations in expression between *IFNG* and genes activated by IFN- $\gamma$  signaling (**Fig. 2B**). *IFNG* expression correlated positively with that of *IDO1*, nitric oxide synthase 2 (*NOS2*), interferon regulatory factor 1 (*IRF1*), and granzymes *GZMB* and *GZMM*, but not programmed death-ligand 1 (*PD-L1*).

These results prompted us to evaluate the impact of *IFNG* expression on the clinical outcomes of AML patients. We computed a prognostic index (PI), as previously published (31), based on expression levels of the 30 DEGs from our NanoString analysis (DataSheet\_page2), which was applied to 149 cases of non-promyelocytic AML from the TCGA project (33). Correlation analyses identified metagenes with co-ordinated regulation (black boxes in **Fig. 2C**), showing that the PI genes clustered with previously published IFN- $\gamma$  signature with prognostic and predictive potential in AML (STM 2020) (34).

Survival analysis revealed that patients whose PI was above the median had significantly shorter overall survival than those with a PI below the median (**Fig. 2D**). Remarkably, only the up-regulated genes contributed to poor survival (Supplementary Fig. S2D, left panel); the down-regulated genes were not prognostic (Supplementary Fig. S2D, right panel).

We assessed whether abnormalities in the expression of the 30 DEGs between IFNG<sup>high</sup> and IFNG<sup>low</sup> groups, as identified by NanoString analysis, might correlate with the mutational status of established prognosticators (*TP53*, *NPM1*, *DNMT3A*, *ASXL1*, *CEBPA*, *RUNX1*, *IDH1/2*, *FLT3-ITD*) in TCGA-AML cases. By default, gene abnormalities are defined as either RNA upregulation or gene deletion/gene amplification. We found a positive correlation between abnormalities in the DEGs and *TP53* mutational status (Supplementary Figure S3).

Overall, these data suggest that  $IFNG^{high}$  and  $IFNG^{low}$  AML samples express distinct gene signatures. Intriguingly, along with genes belonging to inflammatory pathways, high *IFNG* expression also correlated with high expression of immunosuppressive genes induced by IFN- $\gamma$  signaling and associated with a poor clinical outcome.

### **High IFN- $\gamma$ production by AML cells results in increased Tregs in the BM**

We next investigated whether all BM cells synthesize IFN- $\gamma$  or if specific cell populations were responsible. BM mononuclear cells of AML patients (Supplementary Table S1) were stained for CD3, blast cell-associated markers (i.e., CD34, CD33, or CD117), and intracellular IFN- $\gamma$ . Flow cytometry showed that a substantial fraction of CD3<sup>+</sup> cells expressing a blast-surface marker contained IFN- $\gamma$  (**Fig. 3A**). Similar to *IFNG* mRNA data (**Fig. 1A**), there was high inter-patient variability in the fraction of IFN- $\gamma$ <sup>+</sup> AML cells (median, 21.1%; range, 2.1%-67.0%), allowing us to dichotomize at the median into IFN- $\gamma$ <sup>high</sup> and IFN- $\gamma$ <sup>low</sup> groups (**Fig. 3B**, Supplementary S4A, S4B, and S4C). The mean percentages of IFN- $\gamma$ <sup>+</sup> cells in the IFN- $\gamma$ <sup>high</sup> and IFN- $\gamma$ <sup>low</sup> groups were 35.9% and 6.4%, respectively (**Fig. 3B**). This percentage in the IFN- $\gamma$ <sup>high</sup> group was significantly different from that in CD34<sup>+</sup> cells from healthy BM donors. Similar results were obtained by analyzing the IFN- $\gamma$  mean fluorescence intensity (Supplementary Fig. S4B). AML samples classified as IFN- $\gamma$ <sup>high</sup> and IFN- $\gamma$ <sup>low</sup> had similar, low percentages of CD3<sup>+</sup>, CD8<sup>+</sup>, NK cells, and other cell types (**Fig. 3C**). The mean fluorescence intensity (MFI) of the IFN- $\gamma$  signal was not significantly different between the analyzed cell populations (Supplementary Fig. S4D), indicating that AML cells expressed IFN- $\gamma$  at a level comparable to immune cells. Moreover, within each cell population, the fraction of IFN- $\gamma$ <sup>+</sup> cells was associated significantly with group assignment (IFN- $\gamma$ <sup>high</sup> vs. IFN- $\gamma$ <sup>low</sup>) only for AML cells (**Fig. 3D**).

We further investigated the immune cell composition of AML samples according to IFN- $\gamma$  production by AML cells, and we found that the percentage of CD3<sup>+</sup>CD4<sup>+</sup>CD25<sup>+</sup>CD127<sup>low/-</sup> cells (namely Tregs) (35) (Supplementary Fig. S4E) was significantly higher in IFN- $\gamma$ <sup>high</sup> than in IFN- $\gamma$ <sup>low</sup>

and healthy donor samples (**Fig. 3E**). Furthermore, there was a positive correlation between the percentages of Tregs and IFN- $\gamma^+$  AML cells (**Fig. 3F**). Notably, the percentage of CD25<sup>high</sup>CD45RA<sup>-</sup>FOXP3<sup>+</sup> Tregs (Supplementary Fig. S4E), indicated, among Treg subsets, as ‘activated Tregs’ retaining suppressive activity *in vitro* (36) was higher in IFN- $\gamma^{\text{high}}$  than IFN- $\gamma^{\text{low}}$  samples (**Fig. 3G**). Accordingly, a higher percentage of activated Tregs expressing cytotoxic T-lymphocyte antigen (CTLA)-4<sup>+</sup>PD-1<sup>+</sup> (Supplementary Fig. S2E), known to support Treg suppressive functions (37), was observed in IFN- $\gamma^{\text{high}}$  than IFN- $\gamma^{\text{low}}$  samples (Supplementary Fig. S4F). Consequently, the ratios between Tregs and both CD4<sup>+</sup> and CD8<sup>+</sup> T effector cells were higher in IFN- $\gamma^{\text{high}}$  than IFN- $\gamma^{\text{low}}$  samples (Supplementary Fig. S4G). BM-derived Tregs from IFN- $\gamma^{\text{high}}$  AML patients were able to inhibit the proliferation of autologous CD3<sup>+</sup> cells (Supplementary Fig. S4H) and expressed interleukin (IL)-10 (Supplementary Fig. S4I), a fundamental mediator of Treg-mediated suppression(8), implying their functionality.

These data indicate that, among cells from patients’ BM aspirates, AML cells are the main source of IFN- $\gamma$ . IFN- $\gamma^{\text{high}}$  BM samples do not differ in the percentage of the central immune cells (i.e., CD3<sup>+</sup>, CD8<sup>+</sup>, NK cells) compared with IFN- $\gamma^{\text{low}}$  BM samples but are enriched in suppressive Tregs.

### **IFN- $\gamma^{\text{high}}$ AML cells up-regulate IFN- $\gamma$ -related immunosuppressive genes in MSCs**

MSCs are crucial components of the normal and leukemic BM microenvironment and respond to pro-inflammatory stimuli, especially IFN- $\gamma$ , by modifying the immunological landscape (13,14).

With that in mind, we set up an *in vitro* model to investigate interactions between AML cells (IFN- $\gamma^{\text{high}}$  and IFN- $\gamma^{\text{low}}$ ) and AML patient-derived MSCs. For this purpose, two-chamber co-cultures were used. After 4 days of co-culture, IFN- $\gamma^{\text{high}}$  cells maintained significantly higher levels of *IFNG* expression and IFN- $\gamma$  production than IFN- $\gamma^{\text{low}}$  cells (Supplementary Fig. S5A and S5B), while MSCs did not produce IFN- $\gamma$  (Supplementary Fig. S5C and S5D). Moreover, there was a

significantly higher concentration of IFN- $\gamma$  in the conditioned medium from co-cultures with IFN- $\gamma^{\text{high}}$  than IFN- $\gamma^{\text{low}}$  cells (**Fig. 4A**).

We used a similar model to determine if IFN- $\gamma^{\text{high}}$  and IFN- $\gamma^{\text{low}}$  cells have different effects on MSC gene expression. After 24 h of co-culture, compared to MSC monocultures, we detected 82 up-regulated and 12 down-regulated genes in co-cultures involving IFN- $\gamma^{\text{high}}$  cells, and 17 and 10 genes, respectively, in co-cultures with IFN- $\gamma^{\text{low}}$  cells; 14 genes were up-regulated by both conditions (**Fig. 4B**, DataSheet\_page4). Interactions with IFN- $\gamma^{\text{high}}$  cells resulted not only in a greater number of altered genes than with IFN- $\gamma^{\text{low}}$  cells but also a different pattern of gene induction or down-regulation (**Fig. 4C**). Interestingly, MSCs co-cultured with IFN- $\gamma^{\text{high}}$  cells had increased expression of genes encoding chemokines (e.g., *CXCL1*, *CCL5*) implicated in Treg recruitment in solid tumors (38,39) and of *NFKB2* and *RELB* genes that encode key regulators of *IDO1* (40). Importantly, IFN- $\gamma^{\text{high}}$  but not IFN- $\gamma^{\text{low}}$  cells induced MSCs to up-regulate gene sets related to Treg differentiation (**Fig. 4D**, left panel). Indeed, Treg differentiation signature was not significantly enriched in MSC co-cultured with IFN- $\gamma^{\text{low}}$  cells ( $q=0.11$ ) (**Fig. 4D**, right panel). Finally, a set of IFN- $\gamma$ -dependent immune-modulating pathways, including NF- $\kappa$ B, chemokine, and cytokine signaling, was up-regulated in MSCs co-cultured with IFN- $\gamma^{\text{high}}$  cells (Supplementary Table S6). Taken together, these data suggest that IFN- $\gamma$  synthesis and secretion by AML cells skews MSC phenotype towards immunosuppression.

### **IFN- $\gamma$ release by AML cells *in vitro* drives MSCs to induce Tregs via IDO1**

Tregs, the most prominent and fundamental cell population in the BM microenvironment of AML patients (5-8), significantly contribute to creating an immune-suppressive phenotype (9). We found that the percentage of Tregs was significantly higher in IFN- $\gamma^{\text{high}}$  than IFN- $\gamma^{\text{low}}$  samples (**Fig. 3E**). Based on the results on MSC transcriptome modifications after cultures with IFN- $\gamma^{\text{high}}$  cells (**Fig. 4C and D**), we asked whether the release of IFN- $\gamma$  by AML cells induced MSCs to promote Tregs. To this end, we focused on IDO1, widely recognized as the nodal mediator of the IFN- $\gamma$ -regulated

MSC immunomodulatory properties (13). *IDO1* and *IFNG* gene expression were positively correlated in AML samples (**Fig. 2B**), and, among different cytokines, IFN- $\gamma$  was one of the most potent stimuli for IDO1 induction in MSCs (Supplementary Fig. S6A and S6B).

Thus, we evaluated *IDO1* expression in MSCs co-cultured for 4 days with IFN- $\gamma^{\text{high}}$  or IFN- $\gamma^{\text{low}}$  AML cells, distinguished as described above (**Fig. 3A**). We found *IDO1* higher expression with IFN- $\gamma^{\text{high}}$  cells, in comparison with IFN- $\gamma^{\text{low}}$  AML cells, at both mRNA (**Fig. 5A**) and protein levels (**Fig. 5B**, Supplementary Fig. S6C, S6D and S6E). An IFN- $\gamma$ -neutralizing antibody in co-cultures with IFN- $\gamma^{\text{high}}$  cells significantly reduced *IDO1* induction in MSCs co-cultured with IFN- $\gamma^{\text{high}}$  AML cells. Similar results were obtained with an anti-IFN- $\gamma$  receptor antibody (Supplementary Fig. S6F). *IDO1* expression was not upregulated in MSCs co-cultured with IFN- $\gamma^{\text{low}}$  AML cells w/wo anti-IFN- $\gamma$  antibody (**Fig. 5C**).

Next, we asked if IDO1 up-regulation by IFN- $\gamma^{\text{high}}$  cells may drive MSCs to induce Tregs. First, we co-cultured IFN- $\gamma^{\text{high}}$  cells and MSCs and then replaced the IFN- $\gamma^{\text{high}}$  cells with PBMCs: flow cytometry after 7 days showed a significantly higher fraction of CD3<sup>+</sup>CD4<sup>+</sup>CD25<sup>+</sup>FOXP3<sup>+</sup> cells (*bona fide* Tregs) in the PBMCs cultured with IFN- $\gamma^{\text{high}}$  cell-conditioned MSCs than in PBMCs cultured alone (**Fig. 5D**). The addition of an IDO1 inhibitor virtually abrogated Treg induction (**Fig. 5D**). We used a Treg conversion assay to measure the induction of Tregs from CD4<sup>+</sup>CD25<sup>-</sup> cells cultured with IFN- $\gamma^{\text{high}}$  cell-conditioned MSCs. The fraction of Tregs was low in immunomagnetically purified CD4<sup>+</sup>CD25<sup>-</sup> cells cultured alone but increased significantly when these cells were co-cultured with MSCs previously co-cultured with IFN- $\gamma^{\text{high}}$  cells (**Fig. 5E**, Supplementary Fig. S7A). MSCs never conditioned by AML cells or pre-conditioned with IFN- $\gamma^{\text{low}}$  AML cells induced Treg conversion with an efficiency significantly reduced compared with MSCs co-cultured with IFN- $\gamma^{\text{high}}$  AML cells (**Fig. 5E**). The inclusion of an IDO1 inhibitor substantially reduced the Treg conversion stimulated by MSCs co-cultured with IFN- $\gamma^{\text{high}}$  AML cells (**Fig. 5E**,

Supplementary Fig. S7A). Interestingly, IFN- $\gamma^{\text{high}}$  AML cells alone were unable to induce Tregs (**Fig. 5E**). Tregs generated by MSCs pre-conditioned with IFN- $\gamma^{\text{high}}$  AML cells were functional because they significantly inhibited the proliferation of autologous CD3<sup>+</sup> cells (Supplementary Figure S7B and S7C). Finally, in a Treg proliferation assay, CD4<sup>+</sup>CD25<sup>+</sup> cells, obtained after 7 days of culture of PBMCs with MSCs pre-conditioned by IFN- $\gamma^{\text{high}}$  cells, showed a similar proliferation index in comparison with CD4<sup>+</sup>CD25<sup>+</sup> cells obtained when PBMCs were cultured alone (Supplementary Fig. S5D). These results indicate that the Treg increase induced by IFN- $\gamma^{\text{high}}$  cell-conditioned MSCs is not due to Treg proliferation. Altogether, these data suggest that IFN- $\gamma$  secretion by AML cells drives MSCs to induce Treg conversion in an IDO1-dependent manner.

### **IFN- $\gamma$ secretion by AML cells *in vivo* remodels the BM microenvironment by inducing Tregs and favors leukemia cell engraftment**

To gain insight into the effects of AML cell-derived IFN- $\gamma$  on the BM microenvironment, we established a murine model of AML. For this purpose, we chose the C1498 murine leukemia cell line, which expresses the *Ifng* gene (Supplementary Fig. S8A), and we used shRNA interference to knock down this gene's expression (Supplementary Fig. S8B). Cells transfected with non-specific or *Ifng*-specific shRNA vectors (control or shIFN- $\gamma$  cells, respectively) were injected into C57BL/6 mice tibia. Injection of IFN- $\gamma$ -producing control cells resulted in a diffuse interstitial effacement of BM parenchyma (Supplementary Fig. S8C) that was coherent with localization of AML cells (as previously described (41)). After 31 days, mice were sacrificed, and tibiae were flushed to recover BM cells: flow cytometry showed a significantly higher percentage of engraftment in mice that received control than shIFN- $\gamma$  cells (**Fig. 6A**).

Since *Ifng* knockdown did not modify the intrinsic ability of C1498 cells to proliferate (Supplementary Fig. S8D) or survive (Supplementary Fig. S8E), we asked whether IFN- $\gamma$  stimulates leukemic cell engraftment by modifying the BM microenvironment. Flow cytometry of BM cells revealed similar percentages of CD4<sup>+</sup> (Supplementary Fig. S8F, left panel) and CD8<sup>+</sup> cells

(Supplementary Fig. S8F, right panel) but a significantly higher frequency of Tregs in the BM of mice injected with control than shIFN- $\gamma$  cells (**Fig. 6B**). This Treg expansion was paralleled by a significant increase in a population of Tregs expressing OX40, a Treg-associated fitness marker (Supplementary Fig. S8G), and CTLA-4 (Supplementary Fig. S8H), supporting Treg suppressive functions (37). These data suggest that, in AML, high levels of IFN- $\gamma$  within the BM microenvironment increase Tregs concomitantly with leukemic cell engraftment.

Given these results, we investigated whether the *in vivo* reshaping of the BM microenvironment toward Tregs by IFN- $\gamma$ -producing AML cells was due to increased IDO1. Immunohistochemistry on BM sections revealed that IDO1 expression was significantly lower in mice injected with shIFN- $\gamma$  cells than in control (**Fig. 6C and D**). Immunofluorescence revealed that IDO1 expression decreased also in MSCs, identified as  $\alpha$ -smooth muscle actin (SMA)-nestin<sup>+</sup> cells (**Fig. 6E**, quantified in **Fig. 6F**). A similar pattern was obtained for NOS2 (Supplementary Fig. S8I), a downstream target of IFN- $\gamma$  with a critical role in MSC-mediated immunosuppression (42). Consistently, the administration of the IDO1 inhibitor NLG919 to mice inoculated with control cells reduced leukemia cell engraftment (**Fig. 6G**) and BM Tregs (**Fig. 6H**). IDO1 inhibition in the absence of IFN- $\gamma$  signaling did not modify BM Treg frequency (**Fig. 6H**) or leukemia cell engraftment (**Fig. 6G**). Taken together, these results indicate that IFN- $\gamma$  production by AML cells reshapes the BM microenvironment by inducing Tregs through the upregulation of IDO1. The IFN- $\gamma$ -dependent increase in Tregs is positively associated with leukemia cell engraftment, suggesting the induction of an immune-tolerant microenvironment.

## Discussion

The ability of AML cells to shape the BM niche to their advantage is emerging as a hallmark of this cancer (2,3). Our study builds on this concept and demonstrates that the release of IFN- $\gamma$  by AML cells skews the immunological composition of the BM microenvironment toward an

immunosuppressive phenotype, enriched in suppressive Tregs, which correlates with worse clinical outcomes in AML patients.

AML cells produce a wide array of soluble mediators, which help them increase their autonomous growth capacity (43). Our study shows that AML cells have the ability to release IFN- $\gamma$ . In contrast to other tumor models, where increased IFN- $\gamma$  levels have been linked to cytokine production by infiltrating immune cells (44,45), our study found little, if any, contribution to IFN- $\gamma$  secretion by the major immune cell subsets (i.e., CD8<sup>+</sup> and NK cells). Instead, we found that AML cells are the main source of IFN- $\gamma$ . This finding reveals a unique feature of AML where IFN- $\gamma$  production is more likely the result of an intrinsic dysregulation of leukemia cells rather than the consequence of inflammatory BM changes.

Moreover, our results unravel an unexpected tolerogenic role of IFN- $\gamma$  in the context of AML, highlighting its ‘dark side’ in the creation of an immunosuppressive microenvironment. Indeed, in most tumors, IFN- $\gamma$  is known to provide a signal resulting in enhanced anti-tumor immunity (20) and better clinical outcome (21,22). By contrast, in our AML patients’ cohort, both microarray and NanoString analysis revealed an association of high *IFNG* expression with the upregulation of both inflammatory and, interestingly, immunosuppressive genes (e.g., IDO1 and NOS2). These data enabled us to identify a novel immune gene signature based on the 30 DEGs between IFNG<sup>high</sup> and IFNG<sup>low</sup> AML samples and create a prognostic index capable of dissecting AML patients into two groups with highly significant differences in survival. Notably, *IFNG* expression alone does not allow us to stratify AML patients from our cohort or public databases (our unpublished data), suggesting that the gene network of IFN- $\gamma$ -related downstream signals is more relevant for patients’ outcomes. Moreover, our novel IFN- $\gamma$ -based gene signature clusters with a previously published signature based on higher expression of type I and II IFN-related genes predicting chemotherapy resistance and response to immunotherapy in AML (34). Intriguingly, abnormalities in immune genes, which are part of our novel IFN- $\gamma$ -based signature, positively correlate with *TP53* mutational

status. An IDO1-centered gene signature, recently characterized by our group and predictive of AML patient outcome, highlighted a similar correlation (46). To note, *TP53* mutants have been recently described to have higher expression of IFNG and highly immunosuppressive Tregs in the BM (9,47). Altogether, this body of evidence opens a new compelling scenario in which cell-extrinsic pathways, such as IFN $\gamma$ -IDO1 signaling, may co-exist with cell-intrinsic alterations such as *TP53* mutations and contribute to the reshaping of AML immune landscape, leading to worse clinical outcomes. Since our criteria of samples' selection (>80% myeloblasts) may have excluded some relevant AML patient subsets, typically oligoblastic, among which *TP53* mutants, targeted studies will be required to investigate this hypothesis thoroughly.

Increasing evidence indicates that Tregs are involved in creating an immune-tolerant BM microenvironment in AML. A high frequency of Tregs has been correlated with a reduced response to chemotherapy and poor overall survival (7-10). However, the mechanisms by which Tregs are induced within the BM are poorly understood. Moving from the observation that high IFN- $\gamma$  production by AML cells positively correlates with increased Tregs in the BM of AML patients, we found that the silencing of IFN- $\gamma$  expression in AML cells or IDO1 inhibition in mice inoculated with IFN- $\gamma$ -expressing AML cells reduced the Treg frequency *in vivo*. This effect was paralleled by a decrease of IDO1 expression in BM cells. Together with the profound reshaping by AML cells of the BM cell transcriptome according to *IFNG* expression, these data suggest that Treg induction is part of a remodeling of the BM immune microenvironment initiated by AML cells through IFN- $\gamma$  release. In this process, activation of the IDO1 pathway seemed central, corroborating previous reports that demonstrated a crucial role of IDO1 in orchestrating Treg induction in AML (16,48).

A more comprehensive characterization of IFN- $\gamma$  downstream events in the BM microenvironment could be beneficial also in the transplant setting. IFNG<sup>high</sup> samples showed a downregulated expression of MHC class II genes, such as *HLA-DRB1* and *HLA-DQA1*, *CD74* (the invariant chain), and *CIITA* (Fig. 1C). Transcriptional down-regulation of HLA class II molecules has been

recognized as a post-transplantation mechanism of immune evasion and relapse (46,47) and could be overcome by IFN- $\gamma$  treatment (48). Thus, IFN- $\gamma$  expression by AML cells could affect MHC genes' expression differently from exogenous IFN- $\gamma$  addition, but whether IFN- $\gamma$ -dependent Treg induction could be relevant in post-transplant outcomes remains to be investigated.

IFN- $\gamma$  is the most potent inflammatory signal conferring immunosuppressive properties to MSCs (13,14). In particular, after exposure to IFN- $\gamma$ , MSCs become able to induce fully functional Tregs *in vitro* and *in vivo* (11). We found that IFN- $\gamma$  from AML cells altered gene expression in MSCs by up-regulating immune-tolerant and Treg differentiation pathways. Importantly, IFN- $\gamma$  release by AML cells up-regulated MSC expression of IDO1 and its regulators. This observation was made both *in vitro* and *in vivo*. *In vitro*, IFN- $\gamma$  release by AML cells primed MSCs to induce IDO1, which mediates Treg conversion. *In vivo*, silencing of IFN- $\gamma$  expression in AML cells was associated with a decrease of IDO1-expressing MSCs and Tregs. This result is in accordance with the finding of increased numbers of IDO1-expressing MSCs associated with high levels of Tregs in AML patients (49). It is conceivable that cells other than MSCs may participate in this process. In particular, AML cells have been described to increase IDO1 expression and activity after exposure to IFN- $\gamma$  (16,48,50). Accordingly, *in vivo* ablation of IFN- $\gamma$  production by AML cells reduced IDO1 expression, not only in MSCs. Thus, both AML cells and MSCs might contribute to establishing an immune-tolerant microenvironment via IDO1. However, in this work, we observed that, in a Treg conversion assay, AML cell contribution appears reduced if directly compared with that of the MSCs. Altogether, these data suggest that in the induction of Tregs via IDO1, the role of MSCs may be prevailing, although the participation of other cell subsets cannot be ruled out.

In conclusion, this study shows that AML cells' ability to secrete IFN- $\gamma$  enables them to alter the transcriptome of BM cells, leading to an immunosuppressive phenotype where induced Tregs have a prominent contribution. In such process, tolerogenic MSCs, as a key cellular component of BM niche and professional Treg-inducers, are likely to be pivotal. The newly emerging dual face of

IFN- $\gamma$  can be interpreted as part of the complex immune response in cancer, where the broad range of IFN- $\gamma$  actions could depend on the context of tumor specificity, IFN- $\gamma$ -signaling levels, and microenvironment conditions. A greater understanding of the IFN- $\gamma$ -dependent tolerogenic tuning of the BM microenvironment could help provide a rationale for therapies able to overcome immune-modulatory effects on the stromal and immune microenvironment, such as IDO1 inhibitors, and may support the design of new treatments combining the activation of effector cell functions and inhibition of Tregs.

### **Acknowledgements**

This research was supported by FATRO/Foundation Corrado and Bruno Maria Zaini-Bologna, Fabbri1905 and Bologna AIL (Associazione Italiana contro le Leucemie)/Section of Bologna, Associazione Italiana per la Ricerca sul Cancro (IG22204 to S. Sangaletti and IG20654 to A. Curti). M. Ciciarello was supported by the University of Bologna (Alma Idea Junior Grant 2017), the American Society of Hematology (ASH)/Giuseppe Bigi Memorial Award, Marchesini ACT Foundation and Bologna AIL (Associazione Italiana contro le Leucemie)/Section of Bologna with the kind support of Mrs. Marie-Paule Vedrine. B. Bassani is funded by the FIRC-AIRC (Fondazione Italiana per la Ricerca sul Cancro) fellowship "Guglielmina Lucatello e Gino Mazzega". S. Rutella and J. Vadakekolathu are supported by the John and Lucille van Geest Foundation and the School of Science and Technology, Nottingham Trent University, Nottingham, United Kingdom.

## References

1. Yamashita M, Dellorusso PV, Olson OC, Passegué E. Dysregulated haematopoietic stem cell behaviour in myeloid leukaemogenesis. *Nat Rev Cancer* **2020**;20:365-82
2. Ciciarello M, Corradi G, Loscocco F, Visani G, Monaco F, Cavo M, *et al.* The Yin and Yang of the Bone Marrow Microenvironment: Pros and Cons of Mesenchymal Stromal Cells in Acute Myeloid Leukemia. *Front Oncol* **2019**;9:1135
3. Méndez-Ferrer S, Bonnet D, Steensma DP, Hasserjian RP, Ghobrial IM, Gribben JG, *et al.* Bone marrow niches in haematological malignancies. *Nature Reviews Cancer* **2020**;20:285-98
4. Brück O, Dufva O, Hohtari H, Blom S, Turkki R, Ilander M, *et al.* Immune profiles in acute myeloid leukemia bone marrow associate with patient age, T-cell receptor clonality, and survival. *Blood Adv* **2020**;4:274-86
5. Isidori A, Salvestrini V, Ciciarello M, Loscocco F, Visani G, Parisi S, *et al.* The role of the immunosuppressive microenvironment in acute myeloid leukemia development and treatment. *Expert Rev Hematol* **2014**;7:807-18
6. Williams P, Basu S, Garcia-Manero G, Hourigan CS, Oetjen KA, Cortes JE, *et al.* The distribution of T-cell subsets and the expression of immune checkpoint receptors and ligands in patients with newly diagnosed and relapsed acute myeloid leukemia. *Cancer* **2019**;125:1470-81
7. Ustun C, Miller JS, Munn DH, Weisdorf DJ, Blazar BR. Regulatory T cells in acute myelogenous leukemia: is it time for immunomodulation? *Blood* **2011**;118:5084-95
8. Szczepanski MJ, Szajnik M, Czystowska M, Mandapathil M, Strauss L, Welsh A, *et al.* Increased frequency and suppression by regulatory T cells in patients with acute myelogenous leukemia. *Clin Cancer Res* **2009**;15:3325-32
9. Sallman DA, McLemore AF, Aldrich AL, Komrokji RS, McGraw KL, Dhawan A, *et al.* TP53 mutations in myelodysplastic syndromes and secondary AML confer an immunosuppressive phenotype. *Blood* **2020**;136:2812-23
10. Shenghui Z, Yixiang H, Jianbo W, Kang Y, Laixi B, Yan Z, *et al.* Elevated frequencies of CD4<sup>+</sup> CD25<sup>+</sup> CD127<sup>lo</sup> regulatory T cells is associated to poor prognosis in patients with acute myeloid leukemia. *Int J Cancer* **2011**;129:1373-81
11. Yan Z, Zhuansun Y, Chen R, Li J, Ran P. Immunomodulation of mesenchymal stromal cells on regulatory T cells and its possible mechanism. *Exp Cell Res* **2014**;324:65-74
12. Morrison SJ, Scadden DT. The bone marrow niche for haematopoietic stem cells. *Nature* **2014**;505:327-34
13. Krampera M, Cosmi L, Angeli R, Pasini A, Liotta F, Andreini A, *et al.* Role for interferon-gamma in the immunomodulatory activity of human bone marrow mesenchymal stem cells. *Stem Cells* **2006**;24:386-98
14. Meisel R, Zibert A, Laryea M, Gobel U, Daubener W, Dilloo D. Human bone marrow stromal cells inhibit allogeneic T-cell responses by indoleamine 2,3-dioxygenase-mediated tryptophan degradation. *Blood* **2004**;103:4619-21
15. Munn DH, Mellor AL. Indoleamine 2,3-dioxygenase and tumor-induced tolerance. *J Clin Invest* **2007**;117:1147-54

16. Curti A, Trabanelli S, Salvestrini V, Baccarani M, Lemoli RM. The role of indoleamine 2,3-dioxygenase in the induction of immune tolerance: focus on hematology. *Blood* **2009**;113:2394-401
17. Hanahan D, Weinberg RA. Hallmarks of cancer: the next generation. *Cell* **2011**;144:646-74
18. Grivennikov SI, Greten FR, Karin M. Immunity, inflammation, and cancer. *Cell* **2010**;140:883-99
19. de Bruin AM, Voermans C, Nolte MA. Impact of interferon- $\gamma$  on hematopoiesis. *Blood* **2014**;124:2479-86
20. Ivashkiv LB. IFN $\gamma$ : signalling, epigenetics and roles in immunity, metabolism, disease and cancer immunotherapy. *Nat Rev Immunol* **2018**;18:545-58
21. Overacre-Delgoffe AE, Chikina M, Dadey RE, Yano H, Brunazzi EA, Shayan G, *et al.* Interferon- $\gamma$  Drives T. *Cell* **2017**;169:1130-41.e11
22. Fridman WH, Pagès F, Sautès-Fridman C, Galon J. The immune contexture in human tumours: impact on clinical outcome. *Nature Reviews Cancer* **2012**;12:298-306
23. Zaidi MR, Merlino G. The two faces of interferon- $\gamma$  in cancer. *Clin Cancer Res* **2011**;17:6118-24
24. Corradi G, Baldazzi C, Očadlíková D, Marconi G, Parisi S, Testoni N, *et al.* Mesenchymal stromal cells from myelodysplastic and acute myeloid leukemia patients display in vitro reduced proliferative potential and similar capacity to support leukemia cell survival. *Stem Cell Res Ther* **2018**;9:271
25. Simonetti G, Angeli D, Petracci E, Fonzi E, Vedovato S, Sperotto A, *et al.* Adrenomedullin Expression Characterizes Leukemia Stem Cells and Associates With an Inflammatory Signature in Acute Myeloid Leukemia. *Front Oncol* **2021**;11:684396
26. Simonetti G, Padella A, do Valle IF, Fontana MC, Fonzi E, Bruno S, *et al.* Aneuploid acute myeloid leukemia exhibits a signature of genomic alterations in the cell cycle and protein degradation machinery. *Cancer* **2019**;125:712-25
27. Metsalu T, Vilo J. ClustVis: a web tool for visualizing clustering of multivariate data using Principal Component Analysis and heatmap. *Nucleic Acids Res* **2015**;43:W566-70
28. Kuleshov MV, Jones MR, Rouillard AD, Fernandez NF, Duan Q, Wang Z, *et al.* Enrichr: a comprehensive gene set enrichment analysis web server 2016 update. *Nucleic Acids Res* **2016**;44:W90-7
29. Subramanian A, Tamayo P, Mootha VK, Mukherjee S, Ebert BL, Gillette MA, *et al.* Gene set enrichment analysis: a knowledge-based approach for interpreting genome-wide expression profiles. *Proc Natl Acad Sci U S A* **2005**;102:15545-50
30. Livak KJ, Schmittgen TD. Analysis of relative gene expression data using real-time quantitative PCR and the 2(-Delta Delta C(T)) Method. *Methods* **2001**;25:402-8
31. Wagner S, Vadakekolathu J, Tasian SK, Altmann H, Bornhäuser M, Pockley AG, *et al.* A parsimonious 3-gene signature predicts clinical outcomes in an acute myeloid leukemia multicohort study. *Blood Adv* **2019**;3:1330-46
32. Dohner H, Estey E, Grimwade D, Amadori S, Appelbaum FR, Buchner T, *et al.* Diagnosis and management of AML in adults: 2017 ELN recommendations from an international expert panel. *Blood* **2017**;129:424-47
33. Ley TJ, Miller C, Ding L, Raphael BJ, Mungall AJ, Robertson A, *et al.* Genomic and epigenomic landscapes of adult de novo acute myeloid leukemia. *N Engl J Med* **2013**;368:2059-74
34. Vadakekolathu J, Minden MD, Hood T, Church SE, Reeder S, Altmann H, *et al.* Immune landscapes predict chemotherapy resistance and immunotherapy response in acute myeloid leukemia. *Sci Transl Med* **2020**;12
35. Liu W, Putnam AL, Xu-Yu Z, Szot GL, Lee MR, Zhu S, *et al.* CD127 expression inversely correlates with FoxP3 and suppressive function of human CD4+ T reg cells. *J Exp Med* **2006**;203:1701-11

36. Miyara M, Yoshioka Y, Kitoh A, Shima T, Wing K, Niwa A, *et al.* Functional delineation and differentiation dynamics of human CD4<sup>+</sup> T cells expressing the FoxP3 transcription factor. *Immunity* **2009**;30:899-911
37. Chen PP, Cepika AM, Agarwal-Hashmi R, Saini G, Uyeda MJ, Louis DM, *et al.* Alloantigen-specific type 1 regulatory T cells suppress through CTLA-4 and PD-1 pathways and persist long-term in patients. *Sci Transl Med* **2021**;13:eabf5264
38. Wang X, Lang M, Zhao T, Feng X, Zheng C, Huang C, *et al.* Cancer-FOXP3 directly activated CCL5 to recruit FOXP3. *Oncogene* **2017**;36:3048-58
39. Lv M, Xu Y, Tang R, Ren J, Shen S, Chen Y, *et al.* miR141-CXCL1-CXCR2 signaling-induced Treg recruitment regulates metastases and survival of non-small cell lung cancer. *Mol Cancer Ther* **2014**;13:3152-62
40. Puccetti P, Grohmann U. IDO and regulatory T cells: a role for reverse signalling and non-canonical NF-kappaB activation. *Nat Rev Immunol* **2007**;7:817-23
41. Tripodo C, Burocchi A, Piccaluga PP, Chiodoni C, Portararo P, Cappetti B, *et al.* Persistent Immune Stimulation Exacerbates Genetically Driven Myeloproliferative Disorders via Stromal Remodeling. *Cancer Res* **2017**;77:3685-99
42. Sato K, Ozaki K, Oh I, Meguro A, Hatanaka K, Nagai T, *et al.* Nitric oxide plays a critical role in suppression of T-cell proliferation by mesenchymal stem cells. *Blood* **2007**;109:228-34
43. Lotem J, Sachs L. Cytokine control of developmental programs in normal hematopoiesis and leukemia. *Oncogene* **2002**;21:3284-94
44. Takeda K, Nakayama M, Hayakawa Y, Kojima Y, Ikeda H, Imai N, *et al.* IFN- $\gamma$  is required for cytotoxic T cell-dependent cancer genome immunoediting. *Nat Commun* **2017**;8:14607
45. Abiko K, Matsumura N, Hamanishi J, Horikawa N, Murakami R, Yamaguchi K, *et al.* IFN- $\gamma$  from lymphocytes induces PD-L1 expression and promotes progression of ovarian cancer. *Br J Cancer* **2015**;112:1501-9
46. Ragaini S, Wagner S, Marconi G, Parisi S, Sartor C, Nanni J, *et al.* An IDO1-related immune gene signature predicts overall survival in acute myeloid leukemia. *Blood Adv* **2021**
47. Vadakekolathu J, Lai C, Reeder S, Church SE, Hood T, Lourdasamy A, *et al.* TP53 abnormalities correlate with immune infiltration and associate with response to flotetuzumab immunotherapy in AML. *Blood Adv* **2020**;4:5011-24
48. Curti A, Pandolfi S, Valzasina B, Aluigi M, Isidori A, Ferri E, *et al.* Modulation of tryptophan catabolism by human leukemic cells results in the conversion of CD25<sup>-</sup> into CD25<sup>+</sup> T regulatory cells. *Blood* **2007**;109:2871-7
49. Mansour I, Zayed RA, Said F, Latif LA. Indoleamine 2,3-dioxygenase and regulatory T cells in acute myeloid leukemia. *Hematology* **2016**;21:447-53
50. Curti A, Aluigi M, Pandolfi S, Ferri E, Isidori A, Salvestrini V, *et al.* Acute myeloid leukemia cells constitutively express the immunoregulatory enzyme indoleamine 2,3-dioxygenase. *Leukemia*. England2007. p 353-5.

## Figure legends

**Figure 1.** *IFNG* expression in AML samples is highly variable. **A**, Relative expression of *IFNG* mRNA in BM-derived mononuclear cells from 7 healthy donors (HDs) and 61 AML patients at diagnosis. **B**, Relative expression of *IFNG* mRNA in HDs (n=7) and AML samples dichotomized into *IFNG*<sup>low</sup> (n=31) and *IFNG*<sup>high</sup> (n=30) groups at the median. Horizontal red lines indicate the median and interquartile range (HDs vs *IFNG*<sup>low</sup>, \*  $P=0.008$ ; HDs vs *IFNG*<sup>high</sup>,  $P=0.551$ ; *IFNG*<sup>low</sup> vs *IFNG*<sup>high</sup>, \*\* $P<0.001$ ; Kruskal-Wallis-test). **C**, Heatmap of differentially expressed genes ( $|FC|\geq 2.0$  and  $P\leq 0.05$ ) between *IFNG*<sup>high</sup> and *IFNG*<sup>low</sup> AML cells. Columns represent patients. Color changes within rows indicate expression levels relative to the mean for each gene, rescaled on the standard deviation. Genes are ranked according their fold change (from high to low, *IFNG*<sup>high</sup>/*IFNG*<sup>low</sup>) inside each macro-pathway (shown on the right).

**Figure 2.** *IFNG*<sup>high</sup> AML cells express a distinctive inflammatory and immune gene signature correlated to poor overall survival. **A**, Heatmap of differentially expressed genes between *IFNG*<sup>high</sup> and *IFNG*<sup>low</sup> groups ( $|\log_2 FC|>2.0$  and  $P<0.05$ , adjusted  $P$  value, false discovery rate). ClustVis, an online tool for multivariate data clustering (Euclidean distance, complete linkage), was used for data visualization. **B**, Pearson's correlations between NanoString-derived mRNA levels of *IFNG* and *IFNG*-modulated immune-related genes. **C**, Correlogram showing the co-expression of the 30 DEGs between *IFNG*<sup>high</sup> and *IFNG*<sup>low</sup> groups and a previously published RNA-based IFN- $\gamma$  signature indicated as *IFNG* (STM2020) (34) in AML cases (N=149) from the TCGA cohort. The plot was drawn using the *corrplot* package in R. **D**, Kaplan-Meier analysis of overall survival for AML patients (N=149, TCGA cohort) dichotomized according to prognostic index in *PI*<sup>high</sup> group (n=74) and *PI*<sup>low</sup> group (n=75) based on expression levels of the 30 DEGs from our NanoString analysis. Log-rank test.

**Figure 3.** IFN- $\gamma$  expressed by AML cells correlates with the presence of Tregs in the BM. **A**, BM cells co-expressing IFN- $\gamma$  and the indicated blast-specific marker analyzed by flow cytometry

(mean  $\pm$  SEM, n=12; CD34 vs CD33,  $P=0.875$ ; CD34 vs CD117,  $P=0.623$ ; CD33 vs CD117,  $P=0.792$ ; one-way ANOVA, Tukey comparison). **B**, IFN- $\gamma^+$  cells in immune-magnetically purified CD34 $^+$  cells from healthy BM donors (n=4) and in IFN- $\gamma^{\text{high}}$  (n=8) and IFN- $\gamma^{\text{low}}$  samples (n=8) (mean  $\pm$  SEM; \* $P<0.001$ , NS, not significant; one-way ANOVA, Bonferroni correction for multiple comparisons). **C**, Cellular composition of IFN- $\gamma^{\text{high}}$  and IFN- $\gamma^{\text{low}}$  samples by flow cytometry. AML cells (CD34 $^+$ , CD33 $^+$ , or CD117 $^+$ ); NK cells (CD45 $^+$ CD3 $^-$ CD56 $^+$ ). Values are averages of at least 5 samples ( $P>0.05$ , two-way ANOVA, Bonferroni correction for multiple comparisons). **D**, IFN- $\gamma^+$  cells in IFN- $\gamma^{\text{high}}$  (n=7) and IFN- $\gamma^{\text{low}}$  (n=7) groups, by cell type (mean  $\pm$  SEM; \* $P<0.001$ ; two-way ANOVA, Bonferroni correction for multiple comparisons). **E**, Frequencies of Tregs (CD3 $^+$ CD4 $^+$ CD25 $^+$ CD127 $^{\text{low}/-}$  cells) in BM cells of healthy donors (HDs; n=5) and in IFN- $\gamma^{\text{high}}$  (n=4) and IFN- $\gamma^{\text{low}}$  (n=7) samples (mean  $\pm$  SEM; \* $P=0.005$ , \*\* $P=0.040$ ; one-way ANOVA, Tukey comparison). **F**, Correlation between the percentages of Tregs and IFN- $\gamma^+$  cells in BM cells (linear regression). **G**, Activated Tregs (CD45RA $^-$ CD25 $^{\text{high}}$ FOXP3 $^+$  cells) within the CD3 $^+$ CD4 $^+$ CD25 $^+$ CD127 $^{\text{low}/-}$  Treg population, expressed as a percentage of CD4 $^+$  cells, in BM cells of healthy donors (n=5) and in IFN- $\gamma^{\text{high}}$  (n=4) and IFN- $\gamma^{\text{low}}$  (n=7) samples (mean  $\pm$  SEM; \* $P=0.008$ , \*\* $P=0.041$ ; one-way ANOVA, Tukey comparison).

**Figure 4.** IFN- $\gamma^{\text{high}}$  AML cells mold the MSC transcriptome towards an immunosuppressive profile.

**A**, IFN- $\gamma$  levels in conditioned medium from co-cultures of MSCs and IFN- $\gamma^{\text{high}}$  or IFN- $\gamma^{\text{low}}$  cells. Each dot represents the average of one sample analyzed by immunoassay in triplicate (mean  $\pm$  SEM of at least 5 experiments with different samples; \* $P=0.025$ ; unpaired  $t$  test). **B**, Venn diagram showing numbers of genes up-regulated and down-regulated in MSCs co-cultured with IFN- $\gamma^{\text{high}}$  (n=5) or IFN- $\gamma^{\text{low}}$  (n=4) cells with respect to MSC monocultures (n=5). **C**, Heatmap of selected immune response-related genes whose expression in MSCs changed as a result of co-culture with IFN- $\gamma^{\text{high}}$  or IFN- $\gamma^{\text{low}}$  cells. Columns report ratios between a co-culture and its related monoculture. Color scale indicates expression levels relative to the mean for each gene, rescaled on the standard

deviation. Genes are sorted by average linkage hierarchical clustering. **D**, Representative enplots from gene set enrichment analysis of immune tolerance signatures in MSCs co-cultured with IFN- $\gamma^{\text{high}}$  cells (left panel) or IFN- $\gamma^{\text{low}}$  cells (right panel). The illustrated pathway (TREG VS T CONV UP) refers to the up-regulation of Treg differentiation from conventional T cells. NES, normalized enrichment score;  $q$ , FDR  $q$  value.

**Figure 5.** IFN- $\gamma^{\text{high}}$  cells upregulates IDO1 expression in MSCs and increase their capacity to induce Tregs. **A**, qRT-PCR analysis of *IDO1* gene expression in MSCs cultured for 4 days, alone (taken as 1) or with IFN- $\gamma^{\text{high}}$  or IFN- $\gamma^{\text{low}}$  cells (mean  $\pm$  SEM of 5 experiments; \* $P=0.004$ , \*\* $P=0.005$ ; one-way ANOVA, Bonferroni correction for multiple comparisons). **B**, Percentage of IDO1<sup>+</sup> cells analyzed by flow cytometry in MSCs cultured for 4 days, alone or with IFN- $\gamma^{\text{high}}$  or IFN- $\gamma^{\text{low}}$  cells (mean  $\pm$  SEM of 3 experiments; MSCs vs IFN- $\gamma^{\text{high}}$ , \* $P=0.039$ ; MSCs vs IFN- $\gamma^{\text{low}}$ ,  $P=0.581$ ; IFN- $\gamma^{\text{high}}$  vs IFN- $\gamma^{\text{low}}$ ,  $P=0.082$ ; one-way ANOVA, Bonferroni correction for multiple comparisons). **C**, qRT-PCR analysis of *IDO1* expression in MSCs cultured for 6 h, alone or with IFN- $\gamma^{\text{high}}$ / IFN- $\gamma^{\text{low}}$  cells, in the absence or presence of an IFN- $\gamma$ -neutralizing antibody (anti-IFN- $\gamma$ , 20  $\mu\text{g/ml}$ ) (mean  $\pm$  SEM of 3 experiments; MSCs alone vs MSCs+IFN- $\gamma^{\text{high}}$  cells, \* $P=0.001$ ; \*\* $P=0.018$  and \*\*\*  $P=0.002$  vs MSCs+IFN- $\gamma^{\text{high}}$  cells; one-way ANOVA, Tukey correction). **D**, Percentages of Tregs (CD3<sup>+</sup>CD4<sup>+</sup>CD25<sup>+</sup>FOXP3<sup>+</sup> T cells, gated on CD4<sup>+</sup>) in 7-day cultures of PBMCs alone or with MSCs pre-cultured with IFN- $\gamma^{\text{high}}$  cells for 4 days, in the absence or presence of IDO inhibitor (1-methyl-DL-tryptophan, 1 mM) (mean  $\pm$  SEM of 6 experiments; \* $P=0.004$ ; \*\* $P=0.002$ ; one-way ANOVA, Tukey correction). **E**, Percentage of CD4<sup>+</sup>CD25<sup>+</sup>FOXP3<sup>+</sup> cells after 7-day cultures of purified CD4<sup>+</sup>CD25<sup>-</sup> T cells, alone, with MSCs or with MSCs pre-cultured for 4 days with IFN- $\gamma^{\text{high}}$ / IFN- $\gamma^{\text{low}}$  cells, in the absence or presence of IDO inhibitor (1-methyl-DL-tryptophan, 1 mM) (mean  $\pm$  SEM of 5 experiments; \* $P<0.001$ , \*\*  $P=0.005$  vs MSCs + IFN- $\gamma^{\text{high}}$  cells; one-way ANOVA, Tukey correction).

**Figure 6.** IFN- $\gamma$  production by AML cells shapes the BM microenvironment by inducing Tregs *in vivo*. Tibia of C57BL/6 mice were injected with C1498 cells transfected with a vector expressing *Ifng*-specific or non-specific shRNA (shIFN- $\gamma$  or control). After 31 days, BM was flushed to obtain cells for flow cytometry and bone was paraffin-embedded for microscopy. **A**, Engraftment (31 days) of BM cells expressing GFP (control, n=6; shIFN- $\gamma$ , n=7; \* $P=0.011$ ; unpaired  $t$  test). **B**, Frequencies of Tregs (CD4<sup>+</sup>CD25<sup>+</sup>Foxp3<sup>+</sup> cells) gated on CD4<sup>+</sup> cells (control, n=7; shIFN- $\gamma$ , n=7; \* $P<0.001$ ; unpaired  $t$  test). **C**, Immunohistochemistry of IDO1 in BM sections. Magnification  $\times 40$ . **D**, Quantification of IDO1 staining of sections in C. Values are percentages of positive signals (3+ and 2+) in five non-overlapping high-power fields ( $\times 400$ ) per group; \* $P<0.001$ , unpaired  $t$  test. **E**, Immunofluorescence in BM sections of IDO1 (red, Alexa Fluor 568),  $\alpha$ SMA–nestin (green, Alexa Fluor 488). IDO1- $\alpha$ SMA–nestin triple-positive cells are indicated in yellow. Blue, nuclei (DAPI). Magnification 40 $\times$ . Representative arrowed cells are shown magnified in the inserts. **F**, Quantification of IDO1 staining in  $\alpha$ SMA–nestin<sup>+</sup> cells in BM sections shown in C. Values are percentage of positive IDO1 signal in  $\alpha$ SMA–nestin<sup>+</sup> cells, in five non-overlapping high-power fields ( $\times 400$ ) per group (\* $P=0.009$ , unpaired  $t$  test). **G**, Engraftment (31 days) of BM cells expressing GFP (control, n=7; control +IDO1 inhib, n=4; shIFN- $\gamma$ , n=7; shIFN- $\gamma$  + IDO1 inhib, n=5; \* $P=0.004$  vs control; \*\* $P<0.001$  vs control; one-way ANOVA, Tukey comparison). **H**, Frequencies of Tregs (CD4<sup>+</sup>CD25<sup>+</sup>Foxp3<sup>+</sup> cells) gated on CD4<sup>+</sup> cells (control, n=7; control + IDO1 inhib, n=4; shIFN- $\gamma$ , n=7; shIFN- $\gamma$  + IDO1 inhib, n=5; \* $P=0.009$  vs control; \*\* $P<0.001$  vs control; one-way ANOVA, Tukey comparison).

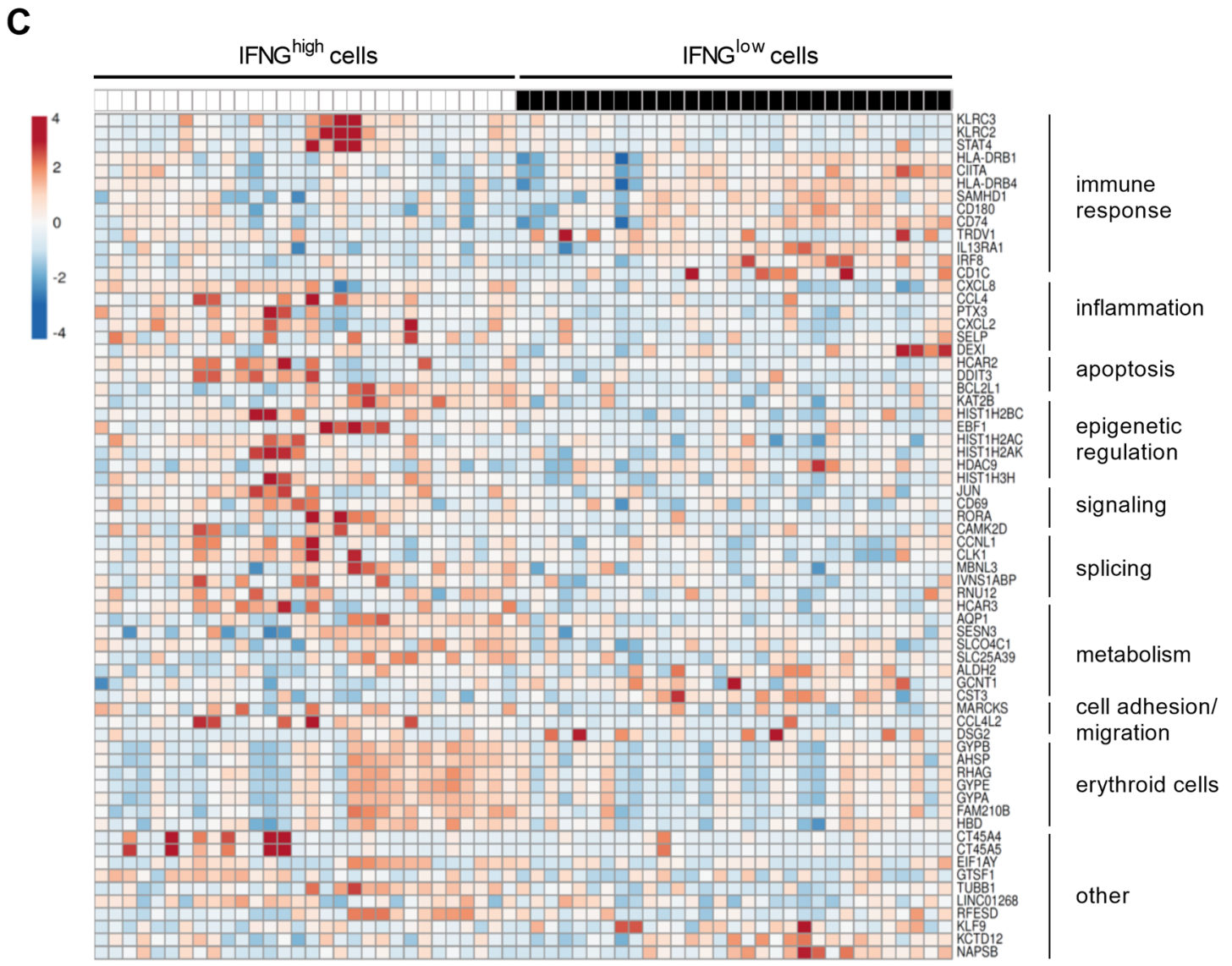
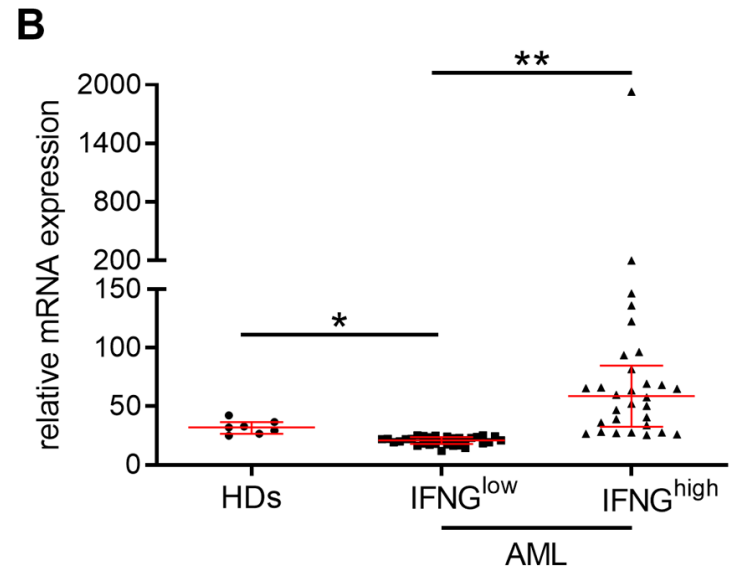
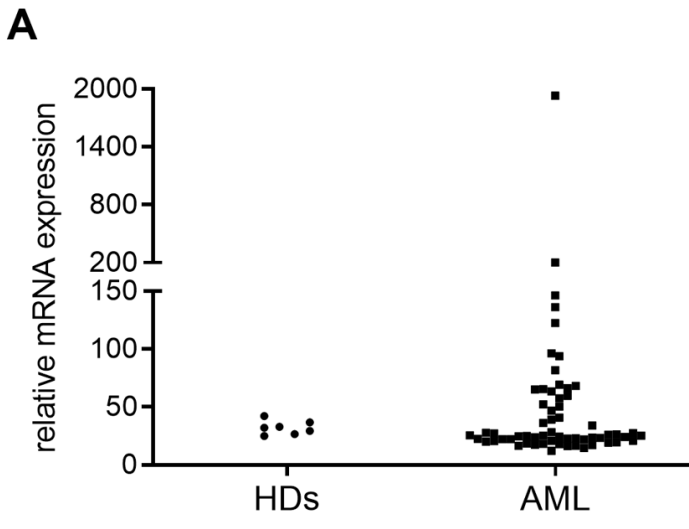


**Figure 1**

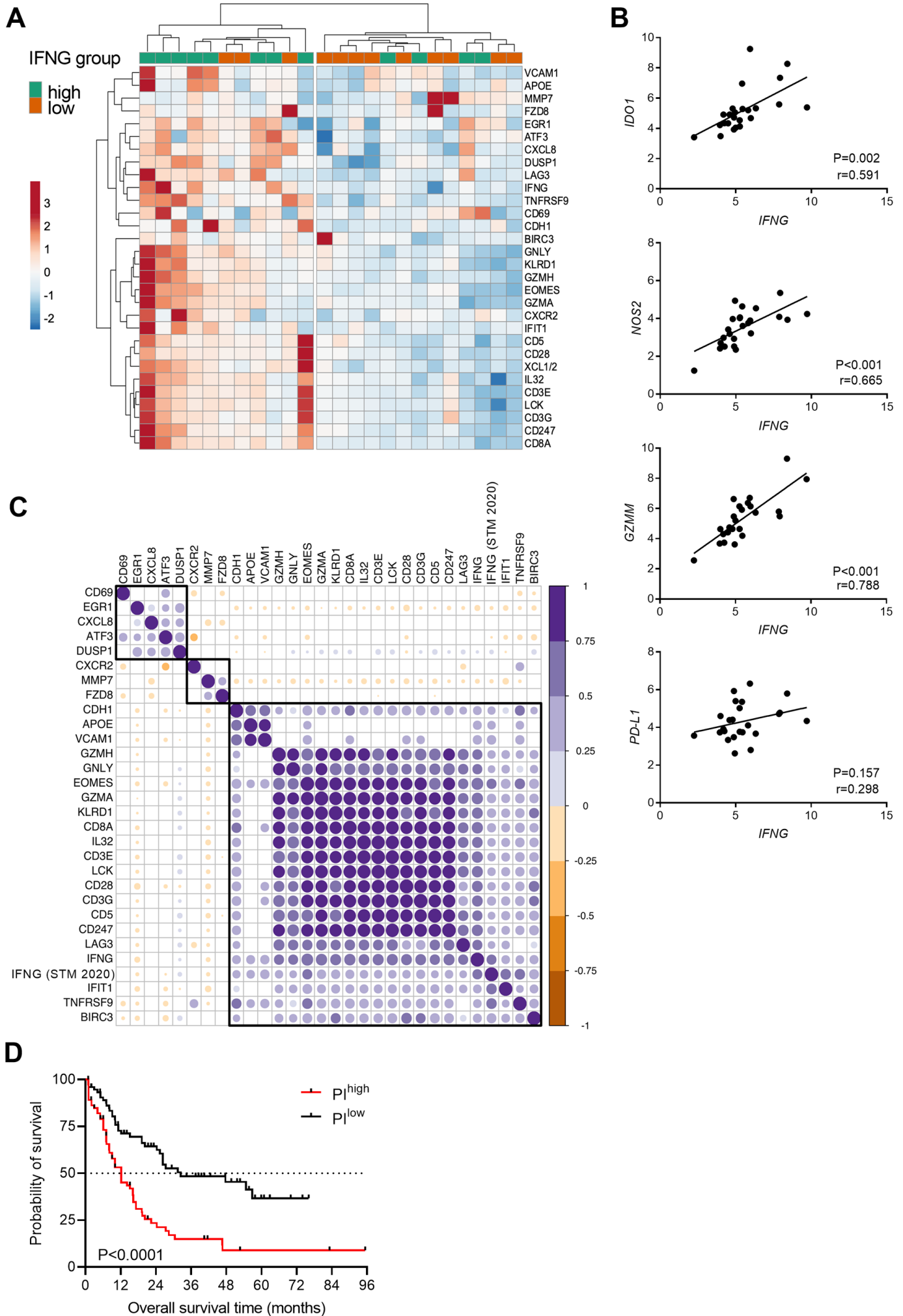
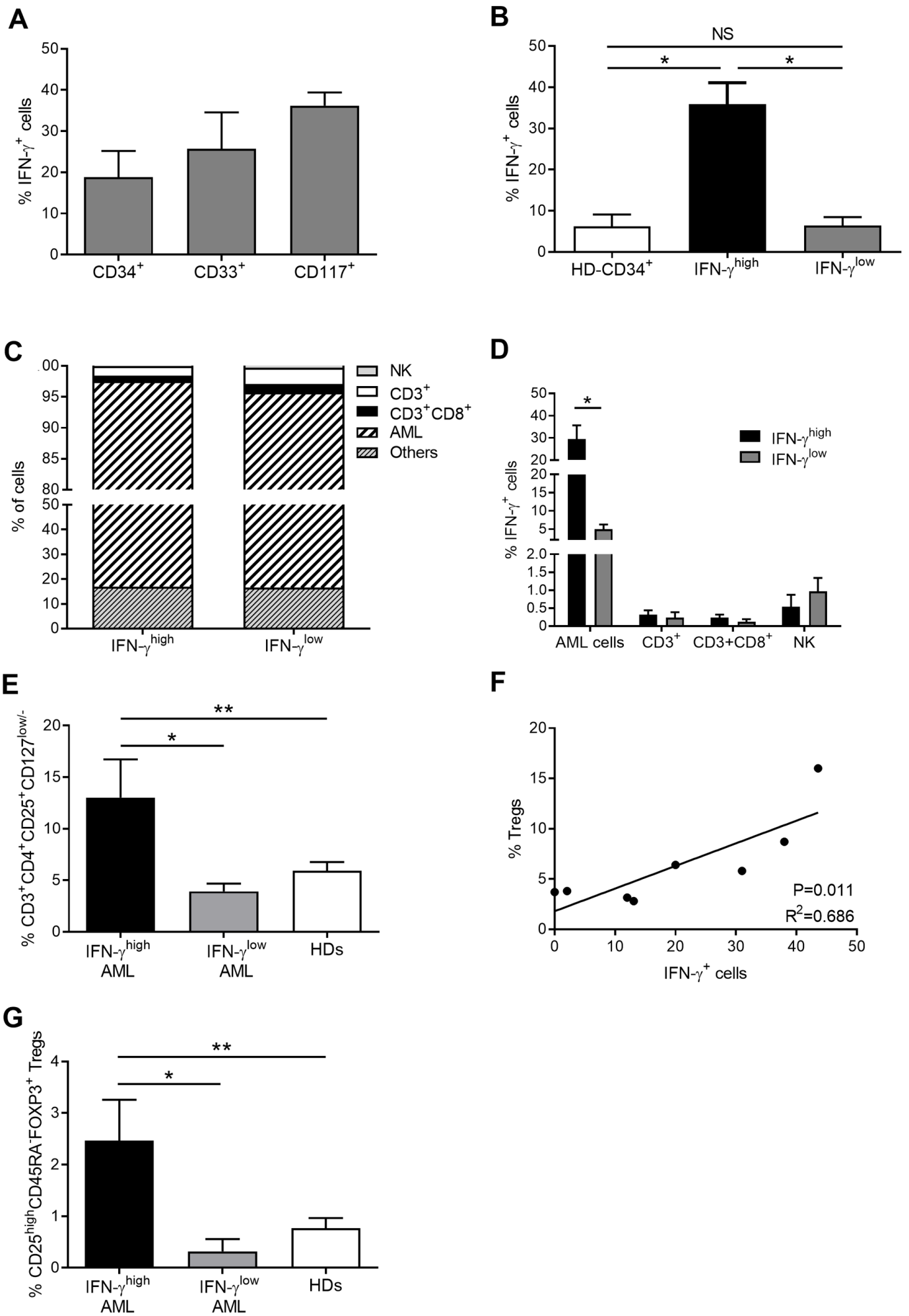
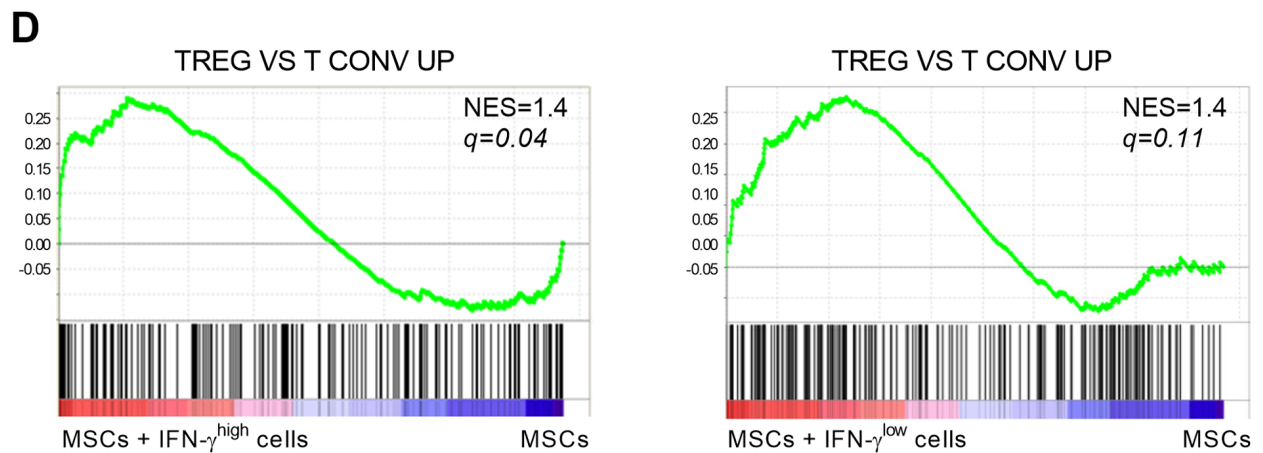
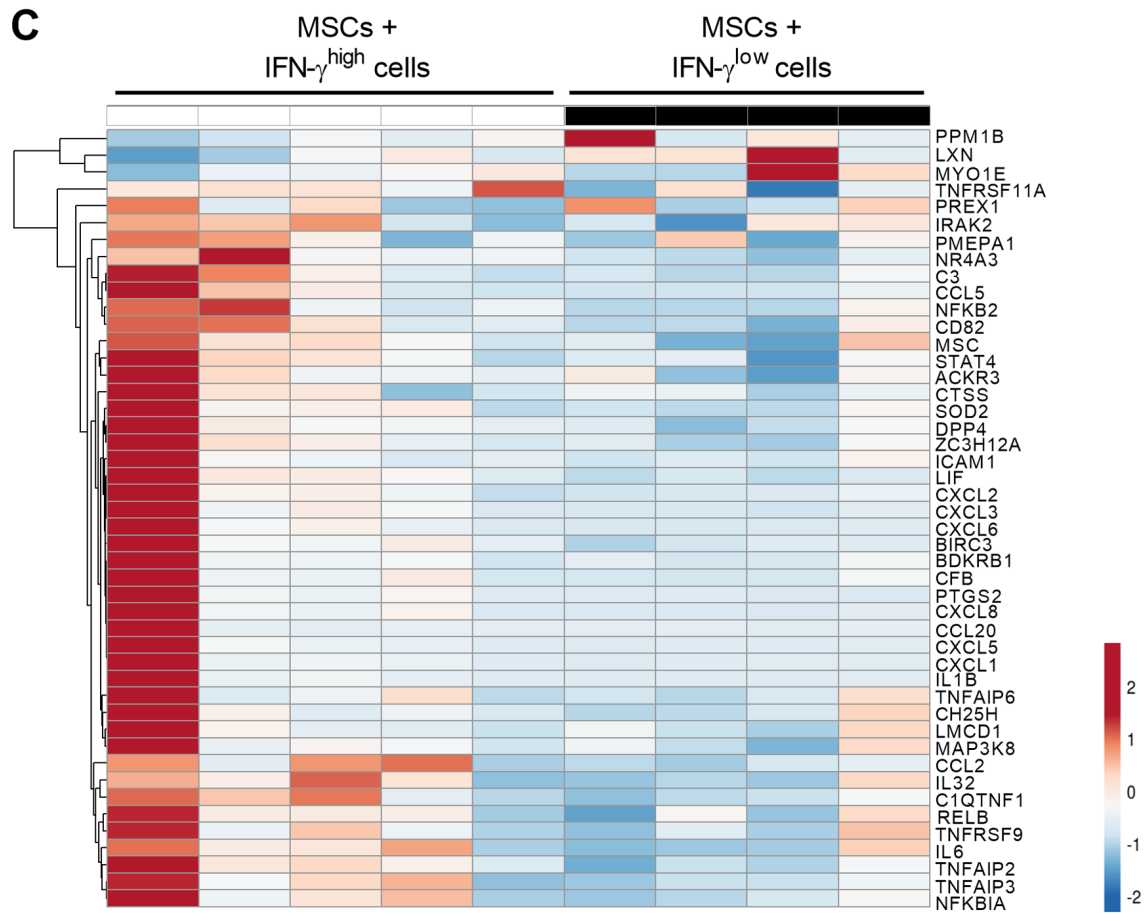
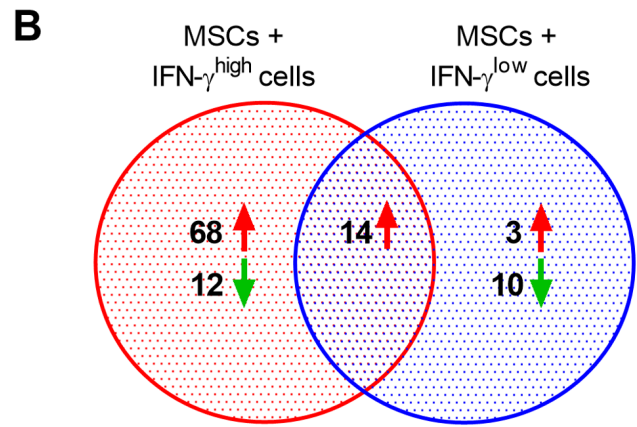
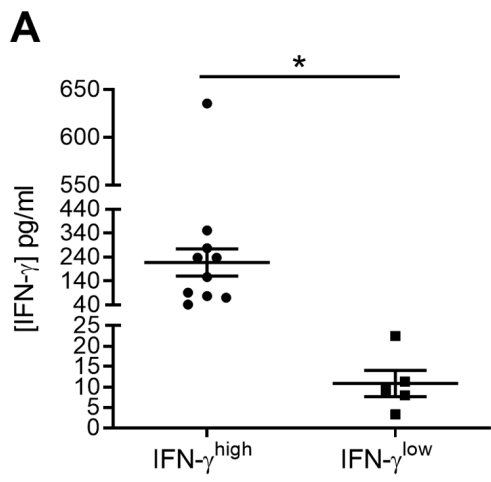


Figure 2



**Figure 3**



**Figure 4**

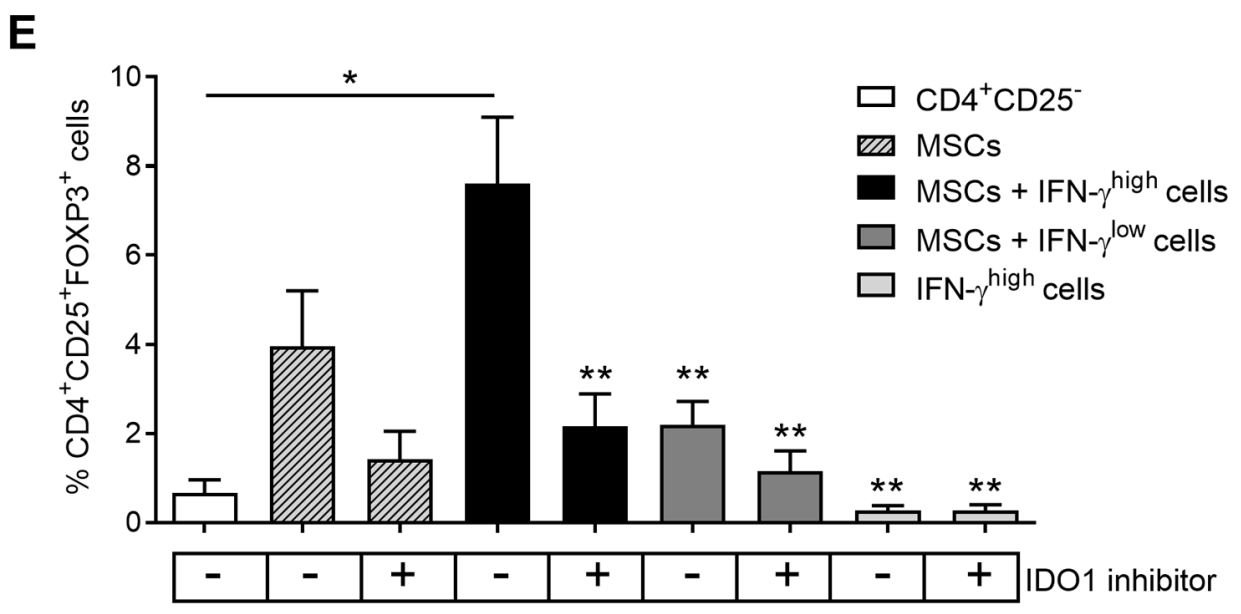
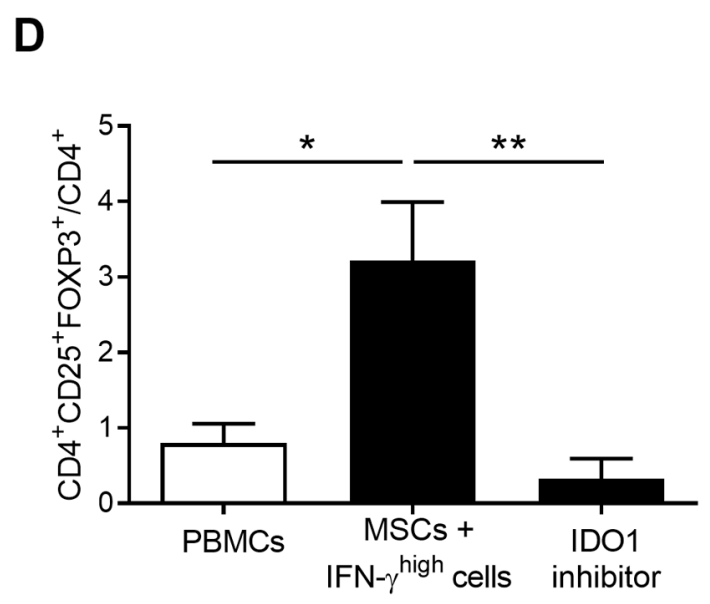
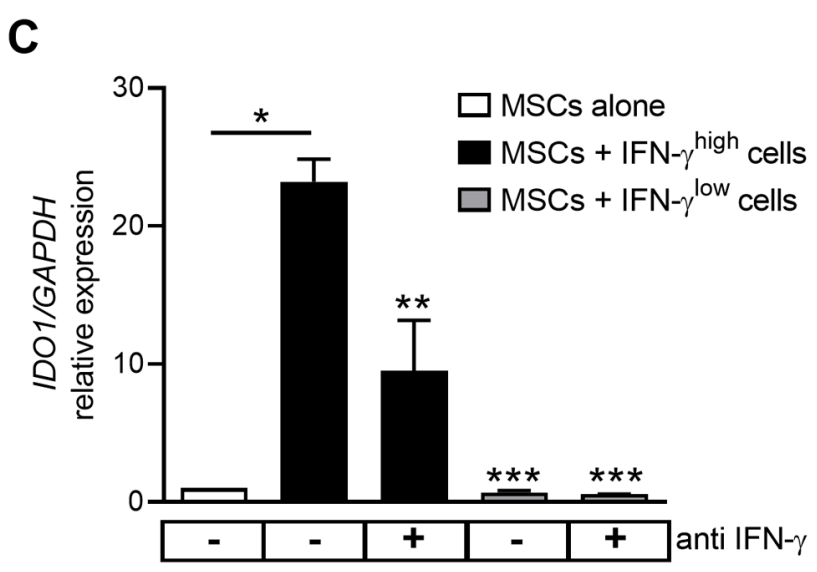
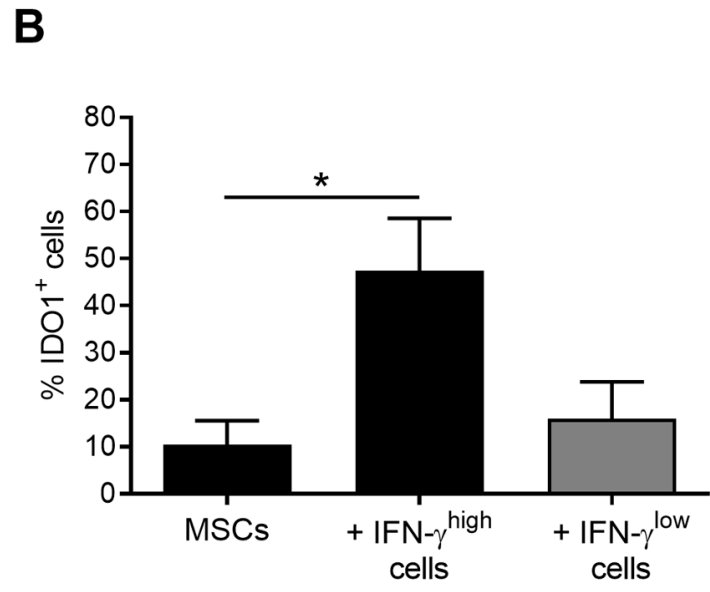
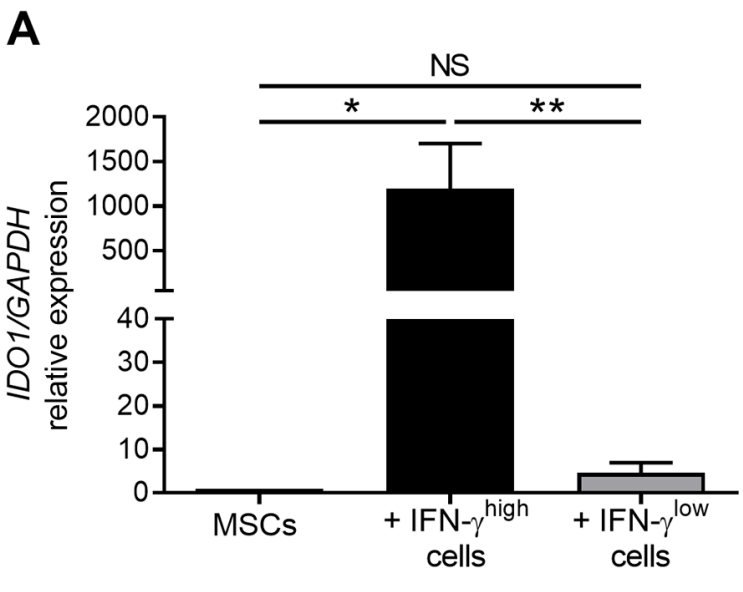


**Figure 5**

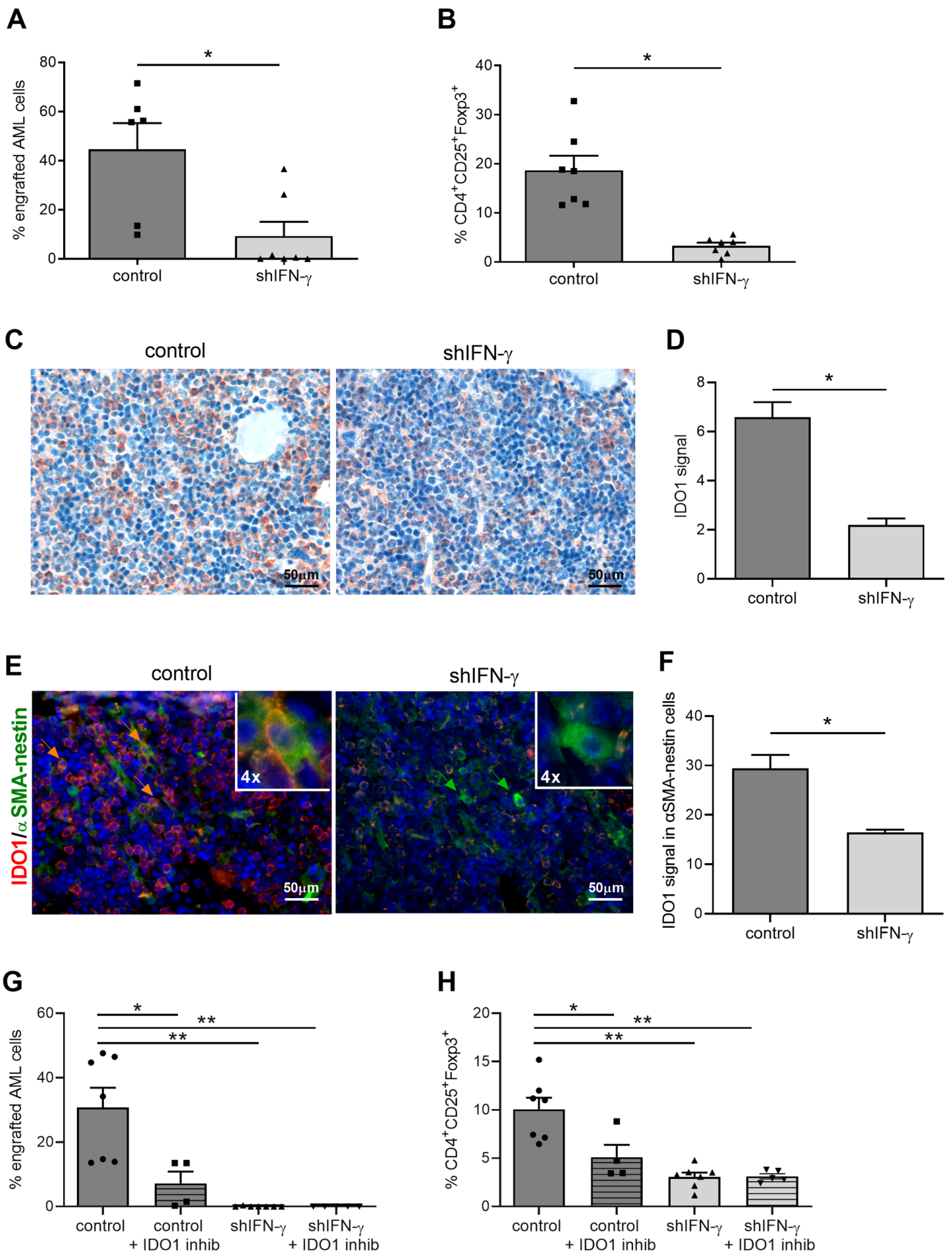


**Figure 6**